

1 Implementation of the ORACLE (v1.0) organic 2 aerosol composition and evolution module into the 3 EC-Earth3-AerChem model 4 5

6 Stylianos Kakavas¹, Stelios Myriokefalitakis², Alexandra P. Tsimpidi³, Vlassis A.
7 Karydis³, and Spyros N. Pandis^{1,4}

8 ¹Institute of Chemical Engineering Sciences, Foundation for Research and
9 Technology Hellas, Patras, Greece

10 ²Institute for Environmental Research and Sustainable Development (IERSD),
11 National Observatory of Athens, Penteli, Greece

12 ³Institute for Energy and Climate Research, IEK-8 Troposphere, Forschungszentrum
13 Jülich GmbH, Jülich, Germany

14 ⁴Department of Chemical Engineering, University of Patras, Patras, Greece
15

16 *Correspondence to:* Spyros N. Pandis (spyros@chemeng.upatras.gr) and Stelios
17 Myriokefalitakis (steliosm@noa.gr).

18
19 **Abstract.** Simulating the composition and evolution of organic aerosol (OA) in Earth
20 System Models (ESMs) presents significant challenges due to the high computational
21 demands of detailed chemical mechanisms. The computationally efficient ORACLE
22 module employs the volatility basis set framework and can simulate secondary
23 organic aerosol (SOA) formation from a range of precursors, including volatile
24 (VOCs), intermediate-volatility (IVOCs), semi-volatile (SVOCs), and low-volatility
25 organic compounds (LVOCs). In this study, a lite configuration of the ORACLE v1.0
26 module (ORACLE-lite) is implemented into the TM5-MP global chemical transport
27 model (CTM), which represents the chemistry-transport component of the EC-Earth3-
28 AerChem ESM. SOA formation from anthropogenic VOCs is neglected to reduce the
29 number of surrogate species and further improve computational efficiency. For the
30 standalone TM5-MP simulation, the global annual mean surface total OA
31 concentration using ORACLE-lite is approximately $1.1 \mu\text{g m}^{-3}$, representing a 25%
32 increase compared to the previous version of the model. The annual atmospheric OA
33 burden also increases by 50%, reaching 3.67 Tg. Corresponding predictions from EC-
34 Earth3-AerChem are slightly higher, with a surface total OA concentration of 1.16
35 $\mu\text{g m}^{-3}$ and an atmospheric burden of 3.83 Tg, representing increases of 30% and

36 60%, respectively, compared to the previous version of the model. Comparison of
37 monthly measured PM_{2.5} OA concentrations from Europe and the US with the
38 corresponding predictions shows that the models bias is reduced by approximately
39 half in the standalone TM5-MP simulation and by a factor of three in EC-Earth3-
40 AerChem when ORACLE-lite is implemented. These enhancements enable more
41 accurate and computationally feasible assessments of the climate impacts of
42 individual organic aerosol components in future ESM studies.

43

44 **1. Introduction**

45 Atmospheric particulate matter (PM) not only affects air quality and human health but
46 also has significant implications for the climate (Monks et al., 2009; Shrivastava et
47 al., 2017; Zhang et al., 2020). Organic aerosol (OA) is a major component of PM
48 contributing between 20% and 90% to the total aerosol mass (Kanakidou et al., 2005;
49 Zhang et al., 2007; Tsimpidi et al., 2025). Since anthropogenic carbonaceous
50 emissions are significant contributors to climate forcing and air pollution (IPCC,
51 2021), it is important to simulate the chemical composition and evolution of OA in
52 Earth System Models (ESMs). This will reduce uncertainties related to aerosols and
53 improve climate predictions.

54 Organic mass is categorized into primary (POA) and secondary organic
55 aerosol (SOA) based on its formation mechanism. Particulate organic mass that is
56 directly emitted into the atmosphere from various sources is referred to as POA. In
57 contrast, SOA is produced in the atmosphere through the oxidation of gas-phase
58 organic compounds. SOA is often the dominant component of OA (Zhang et al.,
59 2007; Crippa et al., 2013; Hu et al., 2016; Nault et al., 2018). However, SOA
60 concentrations are often underestimated in global climate and chemical transport
61 models (Heald et al., 2005; Tsigaridis et al., 2014; Tsimpidi et al., 2016; Bergman et
62 al., 2022). This is partially due to neglected processes in the models (Robinson et al.,
63 2007), such as the evaporation of POA, the oxidation of the resulting vapors in the gas
64 phase and their subsequent condensation into the particle phase, SOA formation from
65 intermediate-volatility organic compounds (IVOCs) and the chemical aging of
66 volatile organic compounds (VOCs). Many studies have shown that the
67 photooxidation of emissions from fossil fuel combustion and biomass burning can
68 lead to the formation of significant SOA concentrations (Kroll and Seinfeld, 2008;

69 Grieshop et al., 2009; Hennigan et al., 2011; Tsimpidi et al., 2017; Ma et al., 2018;
70 Lim et al., 2019; Fang et al., 2021), which is often not accounted for in many ESMs.

71 Climate models usually treat POA and SOA as non-volatile and non-reactive
72 particles that are directly emitted into the atmosphere (Kanakidou et al., 2005;
73 Tsimpidi et al., 2014; Pai et al., 2020). Donahue et al. (2006) introduced the volatility
74 basis set (VBS) framework to capture the changes in OA volatility. This framework
75 describes the partitioning of OA, assuming it is semi-volatile and photochemically
76 reactive and that it is distributed across logarithmically spaced volatility bins. By
77 using this approach, both the emissions of intermediate and semi-volatile primary
78 aerosols, as well as SOA formation and its aging processes can be simulated. This
79 approach has already been implemented in several regional and global chemical
80 transport models (Tsimpidi et al., 2010; Jathar et al., 2011; Shrivastava et al., 2011;
81 Bergström et al., 2012; Woody et al., 2016; Chen et al., 2019; Jiang et al., 2019) and
82 in a few ESMs (Gao et al., 2024; Irfan et al., 2024). Many of these modeling studies
83 have demonstrated improved predictions of OA concentrations by incorporating the
84 VBS framework into their simulations. However, its implementation in large-scale
85 models, such as ESMs, remains limited due to its high computational expense.

86 Tsimpidi et al. (2014) developed the ORACLE module, which is based on the
87 VBS framework, and implemented it in the ECHAM/MESSy Atmospheric Chemistry
88 (EMAC) model (Jöckel et al., 2006). **Compared to a detailed VBS representation with**
89 **explicit volatility bins,** ORACLE reduces the computational cost by utilizing a small
90 number of surrogate OA species by employing a novel lumping method. However, the
91 92 species used in the full configuration of the ORACLE module to describe OA and
92 its volatility are still excessive for ESM simulations increasing significantly the
93 computational cost. To address the computational constraints of ESMs, Tsimpidi et al.
94 (2025) introduced a lite configuration of the ORACLE module (hereafter ORACLE-
95 lite), further reducing the number of species used to describe OA and its volatility
96 from 92 to 18. Although simplifications were made to reduce the computational cost,
97 ORACLE-lite continues to effectively simulate the contributions of low volatility
98 organic compounds (LVOCs), semi-volatile organic compounds (SVOCs), IVOCs,
99 and VOCs to SOA formation (Tsimpidi et al., 2025). ORACLE-lite is recommended
100 for ESM simulations (Riipinen et al., 2025).

101 The aim of this study is to incorporate a computationally efficient OA
102 volatility scheme based on ORACLE-lite into the chemistry-transport component of

Commented [SK1]: Reviewer 1 Comment 2

103 EC-Earth3-AerChem ESM to simulate OA concentrations, composition, and
104 evolution. Section 2 provides an overview of the model, focusing mostly on the new
105 implementations. In particular, we describe the version of the EC-Earth ESM used,
106 the implemented OA volatility scheme, and the conducted simulations. In Section 3,
107 we present the model-derived OA atmospheric concentrations and their evaluation
108 with available observations. Finally, in Section. 4, we discuss the impact of the VBS
109 framework on the simulated OA atmospheric concentrations, and we summarize the
110 global implications of explicitly representing POA emissions in a climate–chemistry
111 model, along with the plans for future model development.

112

113 **2. Model description**

114 **2.1 The EC-Earth3 Earth System Model**

115 The EC-Earth3-AerChem configuration (EC-Earth3-AerChem version 3.5.0) of the
116 EC-Earth3 (van Noije et al., 2021; Döscher et al., 2022~~4~~) has been used for this work.
117 EC-Earth3 contributed to Phase 6 of the Coupled Model Intercomparison Project
118 (CMIP6; Eyring et al., 2016). Its atmospheric general circulation model (GCM) is
119 based on cycle 36r4 of the Integrated Forecast System (IFS), from the European
120 Centre for Medium-Range Weather Forecasts (ECMWF), which includes the H-
121 TESSEL land surface model (Balsamo et al., 2009). The ocean model is version 3.6 of
122 the Nucleus for European Modelling of the Ocean (NEMO; Rousset et al., 2015), with
123 sea ice processes represented by the Louvain-la-Neuve sea ice model (LIM;
124 Vancoppenolle et al., 2009; Rousset et al., 2015). The majority of information
125 exchange and interpolation between modules is managed by the Ocean Atmosphere
126 Sea Ice Soil coupler, version 3 (OASIS3; Craig et al., 2017). EC-Earth3-AerChem
127 includes TM5-MP (Tracer Model 5, Massively Parallel version; Kroll et al., 2005;
128 Huijnen et al., 2010; van Noije et al., 2014; Williams et al., 2017) for the simulation
129 of aerosols and atmospheric chemistry. TM5-MP can be also used as a standalone
130 CTM driven by offline meteorological and surface fields from the ERA-Interim
131 reanalysis, developed by the ~~European Centre for Medium Range Weather Forecasts~~
132 ~~ECMWF~~; (Dee et al., 2011). It simulates the atmospheric life cycle of air pollutants,
133 including emissions, advection, convection, vertical diffusion, and removal by dry and
134 wet deposition, as well as chemical and microphysical transformations. Gas-phase
135 chemistry is described by mCB05, a modified version of the CB05 carbon bond
136 mechanism (Yarwood et al., 2005; Williams et al., 2017). For the gas and particle

Commented [SK2]: Reviewer 1 Comment 3

Commented [SK3]: Reviewer 2 Comment 8

137 equilibrium calculations of $\text{NH}_3/\text{NH}_4^+$ and $\text{HNO}_3/\text{NO}_3^-$, the ISORROPIA-lite model
138 is used (Kakavas et al., 2022) neglecting the effect of organic aerosol water on
139 inorganic aerosol thermodynamics. The organic aerosol water contribution to the total
140 aerosol water is calculated separately, based on Myriokefalitakis et al. (2022). To
141 simulate the composition and evolution of OA the ORACLE-lite module (Tsimpidi et
142 al., 2025) is used.

143 The aerosol population and its evolution are treated by the modal two-moment
144 aerosol model M7 (Vignati et al., 2004). M7 includes four water soluble modes
145 (nucleation, Aitken, accumulation, and coarse) and three insoluble modes (Aitken,
146 accumulation, and coarse). The dry radius size ranges for the aerosol modes are
147 defined as follows: nucleation mode ($r_p < 5$ nm), Aitken mode ($5 < r_p < 50$ nm),
148 accumulation mode ($50 < r_p < 500$ nm), and coarse mode ($r_p > 500$ nm). Particles within
149 each mode are assumed to be internally mixed. Each mode follows a lognormal size
150 distribution with a fixed geometric standard deviation. The M7 model tracks the
151 evolution of both total particle number and the mass of each species within each
152 mode. In this work, we incorporated both POA and SOA into the default soluble POA
153 modes (Aitken, accumulation, and coarse) of the M7 model to track aerosol number
154 distribution. The existing M7 species also include SOA formed from biogenic VOCs
155 (Bergman et al., 2022), along with sulfate, black carbon, sea salt and dust. SOA
156 contributes to the organic aerosol mass within the M7 model, so it affects aerosol
157 growth and particle properties. As cloud droplet activation depends on aerosol size,
158 number, and hygroscopicity, SOA indirectly influences cloud droplet activation in the
159 model through changes in both the aerosol size distribution and composition.
160 Additionally, TM5-MP simulates the concentrations of nitrate, ammonium, and
161 methane sulfonic acid using a bulk aerosol approach.

162 The calculation of aerosol optical properties is based on Mie theory (van Noije
163 et al., 2021). Extinction, single-scattering albedo, and asymmetry factor are derived
164 for each mode using a pre-calculated lookup table. Spectral refractive indices for the
165 different aerosol components are prescribed using input tables from three separate
166 sources. For internally mixed aerosol modes, effective refractive indices are obtained
167 using volume mixing rules derived from effective-medium theory. Organic aerosols,
168 sulfate, sea salt, ammonium, nitrate, methane sulfonic acid, and water are treated as
169 homogeneous mixtures using the Bruggeman mixing rule. In contrast, when black
170 carbon, dust, or both are present, they are treated as inclusions embedded in a

Commented [SK4]: Reviewer 1 Comment 7

Commented [SK5]: Reviewer 1 Comment 6

171 homogeneous host medium, and the Maxwell Garnett mixing rule is applied. More
172 details about TM5-MP and EC-Earth3-AerChem can be found in van Noije et al.
173 (2021) and Myriokefalitakis et al. (2022).

174 2.2 The ORACLE module

175 ORACLE (v1.0) uses fixed, logarithmically spaced saturation concentration
176 bins and assumes bulk equilibrium between the gas and particle phases. The OA mass
177 is then distributed among the size modes (Aitken soluble, accumulation soluble, and
178 coarse soluble) following Pandis et al. (1993), using the dry radius of each size mode
179 from the M7 model. After the bulk equilibrium simulation, the aerosol mass is
180 partitioned across the size modes using a weighting approach that assumes a pseudo-
181 ideal solution for the organic aerosol components. The fraction $f_{i,k}$ of total flux of
182 species i between the gas and aerosol phases that condenses or evaporates from an
183 aerosol mode k is given by:
184

$$185 f_{i,k} = \frac{N_k d_k (c_i - x_{i,k} c_i^*) / (\beta_k + 1)}{\sum_{l=1}^m N_l d_l (c_i - x_{i,l} c_i^*) / (\beta_l + 1)}, \quad (1)$$

186 where N_k and d_k are the number and the mean diameter of particles in mode k ,
187 respectively, and m is the total number of all aerosol modes. The parameter $\beta_k =$
188 $2\lambda/\alpha d_k$, where α is the aerosol accommodation coefficient and λ is the mean free path
189 of air molecules. ORACLE simulates: (i) the partitioning of POA from LVOC
190 emissions, (ii) the partitioning of POA from SVOC emissions and gas-phase oxidation
191 of the remaining vapors, followed by their condensation into the particle phase to
192 form SOA, and (iii) the gas-phase oxidation of IVOC and VOC emissions and the
193 subsequent condensation of the oxidation products to form SOA. The volatility bins
194 are defined by saturation concentration (C^*) ranges of 10^{-2} to 10^{-1} $\mu\text{g m}^{-3}$ for LVOCs,
195 10^0 to 10^2 $\mu\text{g m}^{-3}$ for SVOCs, 10^3 to 10^6 $\mu\text{g m}^{-3}$ for IVOCs, and $>10^6$ $\mu\text{g m}^{-3}$ for
196 VOCs.

197 To further reduce computational expense, we implemented a lite configuration
198 of the ORACLE module (hereafter ORACLE-lite) in the TM5-MP model, which
199 represents the chemistry-transport component of the EC-Earth3-AerChem ESM by
200 introducing a reduced set of surrogate species. This includes POA and primary
201 organic gas (POG) for LVOC emissions, POA and POG for SVOC emissions, and

Commented [SK6]: Reviewer 1 Comment 1;
Reviewer 1 Comment 5

202 POG for IVOC emissions, as well as SOA and secondary organic gas (SOG) formed
203 through the oxidation of SVOC and IVOC emissions by hydroxyl radicals with a rate
204 constant of $1.33 \times 10^{-11} \text{ cm}^3 \text{ molecule}^{-1} \text{ s}^{-1}$. In the present application, SVOCs and
205 IVOCs undergo up to two generations of oxidation, with a 22.5% mass increase in
206 each generation. Assuming an initial OM/OC ratio of 1.2 in ORACLE-lite, this leads
207 to a final OM/OC ratio of up to 1.8, which is within the observed range for
208 oxygenated organic aerosol (OM/OC: 1.8–2.4; Aiken et al., 2008). Note however, that
209 the SOA formation from biogenic VOC emissions (isoprene and monoterpenes) is not
210 treated within ORACLE-lite but is instead simulated—already represented in the
211 models, as described by Bergman et al. (2022). The oxidation of these compounds by
212 ozone and hydroxyl radicals produces SVOCs and extremely low-volatility organic
213 compounds (ELVOCs), which can condense on particles, while Also, SOA formation
214 from anthropogenic VOC emissions is neglected. ORACLE-lite was originally
215 developed for use with the SAPRC family of gas-phase mechanisms. In contrast, EC-
216 Earth3-AerChem employs a modified CB05 chemical mechanism, which uses a
217 different lumping structure for anthropogenic VOCs than that assumed in ORACLE.
218 As a result, the direct inclusion of anthropogenic SOA formation within the current
219 ORACLE-lite framework is complex and requires additional development. This will
220 be the topic of future work. As a result, the number of surrogate species used to
221 represent OA and its volatility in ORACLE-lite was reduced from 18 to 9. An
222 overview of the characteristics of the lite configuration of the ORACLE module used
223 in this study is shown in Table 1.

Commented [SK7]: Reviewer 2 Comment 3

Commented [SK8]: Reviewer 2 Comment 6

Commented [SK9]: Reviewer 1 Comment 4

Commented [SK10]: Reviewer 2 Comment 4

224

225 2.3 Simulations

226 In this study, present-day simulations were performed using atmosphere-only runs of
227 EC-Earth3-AerChem (hereafter referred to as EC-Earth) for the years 2000-2010. In
228 addition, standalone simulations with TM5-MP for the year 2005 driven by ERA-
229 Interim (Dee et al., 2011) were performed. In the EC-Earth simulation, TM5-MP is
230 coupled to the IFS atmospheric dynamics. Sea surface temperature and sea ice
231 concentration fields were prescribed using input files provided through the AMIP
232 interface (Taylor et al., 2000). Consequently, the atmospheric and chemistry modules
233 follow the standard EC-Earth3-AerChem configuration used in CMIP6. The IFS
234 component is configured with a horizontal resolution of T255 (approximately 80 km),

235 91 vertical levels extending up to 0.01 hPa, and a time step of 45 minutes. TM5-MP,
236 in both its standalone and EC-Earth configurations, uses a horizontal resolution of
237 $3^\circ \times 2^\circ$ (longitude \times latitude) and 34 vertical levels extending up to 0.1 hPa (~ 60 km).

238 For this work, two types of simulations were performed for both TM5-MP and
239 EC-Earth: (a) using the default OA representation and emissions, in which OA is
240 treated as non-volatile, non-reactive and emitted exclusively as POA, and (b)
241 incorporating the ORACLE-lite module with modified emissions (hereafter referred
242 to as VBS).

243 In the VBS configuration, the emission factors used to distribute traditional
244 POA emissions into LVOCs and SVOCs are based on the work of Tsimpidi et al.
245 (2025). For fossil fuel combustion sources, emission factors of 0.09 and 0.71 are
246 assigned to LVOCs and SVOCs, respectively. For biomass burning, the
247 corresponding factors are 0.2 for LVOCs and 0.5 for SVOCs. These emissions are
248 assigned to volatility bins with C^* of $10^{-2} \mu\text{g m}^{-3}$ and $10^1 \mu\text{g m}^{-3}$ for LVOCs and
249 SVOCs, respectively (Table 1). Please note that IVOCs exist almost exclusively in the
250 gas-phase (Pandis et al., 2013) and are not fully accounted for in traditional emission
251 inventories, despite their potentially substantial role in SOA formation. Previous
252 studies estimate IVOCs emissions to range from 0.25 to 2.8 times those of traditional
253 POA emissions (Schauer et al., 2002). In this study, we assume that IVOCs emissions
254 are equal to 0.3 times the traditional POA emissions for biomass burning and 1.7
255 times for fossil fuel combustion sources, following the estimates of Tsimpidi et al.
256 (2025). These emissions are assigned to the volatility bin with $C^* = 10^4 \mu\text{g m}^{-3}$.
257 Overall, LVOCs and SVOCs are assumed to be initially emitted in the particle phase
258 as POA, while IVOCs are emitted solely in the gas-phase.

259

260 2.4 Observations

261 To evaluate the impact of the VBS scheme on simulated aerosol concentrations, we
262 compared the models results with monthly surface-level observations of $\text{PM}_{2.5}$ OA
263 concentrations during 2005. We used data from two freely available observational
264 networks: the United States Interagency Monitoring of Protected Visual
265 Environments (IMPROVE; <https://views.cira.colostate.edu/fed/QueryWizard>, last
266 access: 2 June 2025), **which measures aerosols in remote areas of the United States**
267 **and as a result is representative of rural conditions,** and the European Monitoring and
268 Evaluation Project (EMEP; <https://ebas-data.nilu.no/Default.aspx>, last access: 2 June

Commented [SK11]: Reviewer 2 Comment 5

269 2025). For the IMPROVE network, we used monthly OA concentrations from 174
 270 stations while for EMEP, data were available from only 3-4 stations for the simulated
 271 period. Please note that both IMPROVE and EMEP networks measure particulate
 272 organic carbon (OC) instead of total organic mass in the particles. To convert OC to
 273 organic mass, we applied a constant factor. For the IMPROVE network, the suggested
 274 factor equals to 1.8 (Pitchford et al., 2007). For EMEP, we followed the IMPROVE
 275 network recommendation and assumed a factor of 1.8 for EMEP stations to maintain
 276 consistency. The OC measurements at the Ispra (Italy) station of EMEP are
 277 systematically high (reaching up to 22 $\mu\text{g m}^{-3}$ in winter), which strongly influences
 278 the multi-site monthly mean due to the limited number of available stations for 2005.
 279 For this reason, and to avoid the average being dominated by a single site, Ispra was
 280 excluded from the statistical analysis. Due to the limited availability of measurements
 281 in Europe during 2005, we also used monthly OA concentrations from EMEP during
 282 2010, when data from 8 stations were available.

Commented [SK12]: Reviewer 2 Comment 2

Commented [SK13]: Reviewer 2 Comment 2

Commented [SK14]: Reviewer 1 Comment 8

Commented [SK15]: Reviewer 2 Comment 2

284 2.5 Models performance

285 To evaluate the models' performance, specific statistical metrics were calculated for
 286 both configurations of TM5-MP and EC-Earth simulations. These include mean bias
 287 (MB), mean absolute gross error (MAGE), normalized mean bias (NMB), normalized
 288 mean error (NME), and root-mean-square error (RMSE) defined as follows:

$$MB = \frac{1}{N} \sum_{i=1}^N (P_i - O_i) \quad (2)$$

$$MAGE = \frac{1}{N} \sum_{i=1}^N |P_i - O_i| \quad (3)$$

$$NMB = \frac{\sum_{i=1}^N (P_i - O_i)}{\sum_{i=1}^N O_i} \quad (4)$$

$$NME = \frac{\sum_{i=1}^N |P_i - O_i|}{\sum_{i=1}^N O_i} \quad (5)$$

$$RMSE = \left[\frac{1}{N} \sum_{i=1}^N (P_i - O_i)^2 \right]^{1/2} \quad (6)$$

289 where P_i is the predicted OA concentration, O_i is the observed OA value at the same
 290 monthly averaged time, and N is the total number of measurements used for the
 291 comparison.

292 NME (in %) and MAGE (in $\mu\text{g m}^{-3}$) measure the total difference between
293 model predictions and observations, including both bias and scatter. In contrast, NMB
294 (in %) and MB (in $\mu\text{g m}^{-3}$) specifically reflect systematic errors. RMSE (in $\mu\text{g m}^{-3}$)
295 combines both the variability (scatter) and bias of the predictions into a single metric.
296 Because NME and MAGE include bias effects, their values are typically equal to or
297 greater than those of NMB and MB. When NME and NMB (or MAGE and MB) are
298 similar in magnitude, most of the error is due to bias. However, if NME and MAGE
299 are substantially larger than NMB and MB, this indicates that scatter also contributes
300 significantly to the discrepancy between predictions and observations.

301

302

303

304 2.6 Emissions

305 The annual present-day emissions used in ~~both online and offline simulations of the~~
306 ~~chemistry transport component of EC-Earth (TM5-MP)~~ with the VBS configuration
307 are shown in Fig. 1. In the default OA configuration, particulate organic matter is
308 emitted exclusively as POA (Fig. S1; 52.4 Tg yr^{-1}) and is assumed to have constant
309 carbon content, expressed as the ratio of total OA mass to the mass of the carbon it
310 contains. This ratio is used to convert POA emissions, typically expressed as organic
311 carbon (OC) mass to OA mass. In this study, a ratio of 1.6 is applied across all POA
312 sources based on previous works (Turpin and Lim, 2001; Reid et al., 2005; Aiken et
313 al., 2008; van Noije et al., 2021). In the VBS configuration, emissions are distributed
314 into three volatility bins based on the emission factors described in Section 2: LVOCs
315 (7.6 Tg yr^{-1}), SVOCs (31.8 Tg yr^{-1}), and IVOCs (53.1 Tg yr^{-1}) (see also Table 2).
316 LVOCs and SVOCs represent POA emissions, which are lower in total than in the
317 default OA configuration because a portion of the traditional organic mass emissions
318 is reassigned to IVOCs. ~~The corresponding annual mean emissions used for the EC-~~
319 ~~Earth simulation are shown in Fig. 2.~~ The emissions are higher in regions such as
320 China, India, Bangladesh, southern Africa, and South America. Emissions from
321 shipping are also present over oceanic regions.

322

323 3. Results

324 3.1 Budget calculations

Commented [SK16]: Reviewer 1 Comment 9

Commented [SK17]: Reviewer 1 Comment 9

325 This section presents the global budgets, atmospheric burdens, and lifetimes of
326 OA components from EC-Earth and standalone TM5-MP simulations during 2005
327 using the VBS configuration (Table 1). For completeness, SOA from biogenic VOCs
328 (bSOA-v) is also included.

329 In the standalone TM5-MP simulation for 2005, SOA production from SVOCs
330 (SOA-sv) and IVOCs (SOA-iv) is 19.83 Tg yr^{-1} and 37.02 Tg yr^{-1} , respectively. The
331 total annual SOA production is $109.19 \text{ Tg yr}^{-1}$. This value falls within the range of
332 $50\text{-}380 \text{ Tg yr}^{-1}$ of Spracklen et al. (2011) and is close to their best estimate of 140 Tg
333 yr^{-1} . The relative contributions to the annual SOA production are 18.2% from
334 SVOCs, 33.9% from IVOCs, and 47.9% from biogenic VOCs. Anthropogenic SOA
335 production is higher near source regions (Fig. 23), with hotspots in South America,
336 southern Africa, India, Bangladesh, and China. Seasonally, the production of SOA-sv
337 is higher in summer (Fig. S2), whereas SOA-iv production peaks in winter, especially
338 over India, China, and Central Africa (Fig. S3). This seasonal trend will be discussed
339 further in the next section.

340 In the EC-Earth simulation, the annual mean production for 2000-2010 of
341 SOA-sv and SOA-iv is $19.62 \pm 1.67 \text{ Tg yr}^{-1}$ and $38.28 \pm 7.32 \text{ Tg yr}^{-1}$, respectively
342 (Table 2; Fig. 24), with a total SOA production of $109.22 \pm 10.23 \text{ Tg yr}^{-1}$. The
343 contributions to total SOA production are 18% from SVOCs, 35% from IVOCs, and
344 47% from biogenic VOCs. Annual (Fig. S4) and seasonal (Figs. S5 and S6) SOA
345 production indicate no significant differences between the TM5-MP and EC-Earth
346 simulations during 2005. Minor discrepancies arise from differences in meteorology,
347 which is predicted in EC-Earth but prescribed from reanalysis in the TM5-MP
348 simulation.

349 The contributions to the annual atmospheric burden of total OA (3.67 Tg) in
350 the standalone TM5-MP simulation are 18.7% from POA, 16.4% from SOA-sv,
351 32.9% from SOA-iv, and 32% from bSOA-v. Compared to the default simulation, in
352 which SOA is produced only from biogenic VOCs and all anthropogenic OA is
353 treated as POA, the annual atmospheric burden of total OA increased by
354 approximately 50% in the VBS simulation. In EC-Earth, the annual mean atmospheric
355 burden using the VBS configuration is 60% higher than in the default configuration,
356 reaching $3.83 \pm 0.21 \text{ Tg}$. The respective contributions are 19.3% from POA, 15.9%
357 from SOA-sv, 34% from SOA-iv, and 30.8% from bSOA-v.

Commented [SK18]: Reviewer 1 Comment 9

Commented [SK19]: Reviewer 1 Comment 9

358

359 3.2 Atmospheric concentrations

360 The annual mean surface concentrations of POA, SOA-sv, SOA-iv, and bSOA-v in
361 the standalone TM5-MP simulation with the VBS configuration are shown in Fig. 34.

362 POA levels are higher than those of SOA-sv and SOA-iv especially in regions like
363 India and China with higher LVOC and SVOC emissions. Our simulations indicate
364 that the emitted POA undergoes evaporation and is subsequently oxidized by
365 hydroxyl radicals in the gas phase, leading to the formation of SOA-sv through re-
366 condensation. This is consistent with recent experimental studies especially for
367 biomass burning emissions (e.g., Sengupta et al., 2020; Fang et al., 2021). Biomass
368 burning emissions from residential heating are typically higher during winter, and the
369 lower temperatures enhance partitioning to the particle phase, leading to increased
370 POA concentrations, especially in regions such as China, Bangladesh, Central Africa
371 and India (Fig. S7).

372 The annual mean concentrations of SOA-sv are lower than those of POA, as
373 only a fraction of POA evaporates, undergoes photooxidation, and subsequently
374 condenses into the particle phase. The oxidation of IVOCs, producing lower-volatility
375 products, also contributes to SOA-sv formation. Please note that in ORACLE-lite, the
376 volatility bin representing SOA-sv corresponds to a C^* value of $10^{-2} \mu\text{g m}^{-3}$,
377 indicating low volatility and a predominant presence in the particle phase. The higher
378 SOA-sv concentrations predicted during summer compared to winter (Table S1; Fig.
379 S8) are due to the higher summer temperatures promoting POA evaporation, and the
380 increased sunlight which enhances subsequent photooxidation and formation of SOA.

381 Higher annual mean concentrations of SOA-iv compared to SOA-sv are
382 predicted, primarily due to the higher emissions of IVOCs (Table 1; Fig. 1) and the
383 different formation mechanism. IVOCs can directly undergo oxidation by hydroxyl
384 radicals, producing lower-volatility products that subsequently condense into the
385 particle phase. Predicted SOA-iv concentrations are higher in winter than in summer
386 (Table S1), particularly in regions such as China, India, Bangladesh, and Europe (Fig.
387 S9). This is attributed to increased biomass burning emissions in these regions and
388 lower temperatures, which enhance partitioning of the semi-volatile OA components
389 into the particle phase. However, in regions such as South America and southern
390 Africa, where major rainforests like the Amazon and Congo Basin are located, SOA-
391 iv concentrations are higher during summer due to wildfires.

Commented [SK20]: Reviewer 1 Comment 9

392 The annual mean surface concentrations of total OA in the standalone TM5-
393 MP simulation with the VBS configuration are shown in Fig. 45. Higher
394 concentrations are predicted in regions with higher precursor emissions, while as
395 altitude increases the concentrations of OA decrease as expected, with higher
396 concentrations between 15° S and 45° N (Fig. 45b). At higher altitudes, SOA
397 concentrations are higher compared to POA, because organic gases can be efficiently
398 transported upward and oxidized, leading to the formation of lower-volatility SOA
399 (Fig. S10). Additionally, SOA formed at these altitudes tends to have a longer
400 atmospheric lifetime, as it is less affected by wet and dry deposition processes
401 (Tsimpidi et al., 2014).

Commented [SK21]: Reviewer 1 Comment 9

402 The VBS configuration predicts significantly higher annual mean total OA
403 concentrations (by up to 100%) compared to the default TM5-MP configuration,
404 particularly in regions such as India, China, and northern Africa (Fig. 45c).
405 Significant increases are also predicted over oceanic regions, including the Indian,
406 Atlantic and Pacific Oceans. In addition to S/IVOC emissions from shipping (Fig. 1),
407 this increase is largely driven by the long-range transport of IVOCs, which
408 contributes to SOA-iv formation far from emission sources (Aiken et al., 2009;
409 Hildebrandt et al., 2010). This is further supported by the higher increases in total OA
410 concentrations predicted in these regions during winter compared to summer (Fig.
411 S11), attributed to higher SOA-iv levels in the colder season (Fig. S9). At higher
412 altitudes, the VBS configuration in general predicts higher OA concentrations than the
413 default configuration, particularly between 0° and 45°N (Fig. 45d). However, in the
414 uppermost levels of the model, the default configuration predicts higher OA
415 concentrations. Nevertheless, in both simulations, these values are extremely low
416 (below 0.001 $\mu\text{g m}^{-3}$), rendering the absolute differences negligible.

Commented [SK22]: Reviewer 1 Comment 9

Commented [SK23]: Reviewer 1 Comment 9

Commented [SK24]: Reviewer 1 Comment 9

417 The annual mean surface concentrations of POA and SOA in the EC-Earth
418 simulation with the VBS configuration for 2000-2010 are shown in Fig. 56. Similar to
419 the TM5-MP simulation, higher SOA concentrations than POA are predicted. With
420 increasing altitude, SOA concentrations remain higher than POA because organic
421 gases are efficiently transported upward and oxidized, producing lower-volatility
422 SOA. However, compared to the TM5-MP simulation, there are some differences in
423 the global distribution of the annual mean surface total OA for 2005 (Fig. S12). More
424 specifically, in regions such as South America, Africa, India, and China, EC-Earth
425 predicts higher total OA concentrations (up to 4 $\mu\text{g m}^{-3}$) during 2005 due to the higher

Commented [SK25]: Reviewer 1 Comment 9

426 production of SOA-iv. There are also regions such as Europe in which TM5-MP
427 predicts higher total OA concentrations than EC-Earth. At higher altitudes, TM5-MP
428 in general predicts higher OA concentrations than EC-Earth, except in the region
429 between 5° S and 10°N up to 600 hPa (Fig. S12). However, in all cases, the
430 differences are lower than 0.5 $\mu\text{g m}^{-3}$. These discrepancies stem from differences in
431 meteorology since EC-Earth uses meteorology predicted by IFS, while TM5-MP
432 relies on prescribed reanalysis data. More specifically, in these regions, either lower
433 predicted temperatures or lower precipitation rates in EC-Earth affect OA
434 concentrations through partitioning and deposition, respectively (Fig. S13).

435 Overall, higher concentrations of OA are predicted by both models in regions
436 such as India, South America, southern Africa, and China, where precursor emission
437 levels are higher. The annual global mean surface concentration of total OA in the
438 TM5-MP simulation using the VBS configuration is 1.07 $\mu\text{g m}^{-3}$, corresponding to an
439 increase of 25% relative to the default configuration. In EC-Earth, the corresponding
440 annual global mean surface concentration is 1.16 $\mu\text{g m}^{-3}$, representing an increase of
441 30% relative to the default configuration. The contributions of individual OA
442 components to the annual global mean surface concentration of OA are 29.9% from
443 POA, 13.1% from SOA-sv, 29% from biogenic SOA, and 28% from SOA-iv. This
444 highlights the substantial role of IVOCs in contributing to total OA, despite their
445 omission from traditional emission inventories. Additionally, our simulations indicate
446 that temperature influences the partitioning of oxidized IVOC products into the
447 particle phase, with lower temperatures favoring this process. In contrast, oxidized
448 SVOC products are treated as low-volatility compounds in the ORACLE-lite module
449 and predominantly remain in the particle phase under typical atmospheric conditions.

450

451 3.3 Models evaluation

452 Figure [7-6](#) shows the comparison between predicted $\text{PM}_{2.5}$ OA concentrations and
453 corresponding measurements for both the TM5-MP and EC-Earth simulations during
454 2005. Each point on the scatterplot represents a monthly average value at a specific
455 monitoring station. Compared to the default configuration, the VBS configuration of
456 TM5-MP predicts higher OA concentrations at all stations, with model results
457 generally falling closer to the 1:1 line. More specifically, in both TM5-MP
458 simulations, OA concentrations are generally underpredicted at the examined stations,

Commented [SK26]: Reviewer 1 Comment 9

459 as indicated by negative MB and NMB values (Table 3). However, the VBS
460 configuration reduces this underprediction by approximately half (MB = $-0.28 \mu\text{g m}^{-3}$,
461 NMB = -13.2%) compared to the default configuration (MB = $-0.57 \mu\text{g m}^{-3}$,
462 NMB = -27.1%). Additionally, both NME and RMSE values, which are relatively
463 low in the default simulation (NME = 42% , RMSE = $1.57 \mu\text{g m}^{-3}$), improve further in
464 the VBS simulation (NME = 38.9% , RMSE = $1.5 \mu\text{g m}^{-3}$), indicating reduced scatter.
465 The same applies for MAGE, which decreased from $0.89 \mu\text{g m}^{-3}$ in the default
466 simulation to $0.82 \mu\text{g m}^{-3}$ in the VBS simulation. The corresponding EC-Earth
467 metrics for 2005 for both configurations are also shown in Table 3. EC-Earth also
468 underpredicts OA concentrations at the examined stations. However, the VBS
469 configuration of EC-Earth reduces the underprediction by approximately a factor of
470 three (MB = $-0.17 \mu\text{g m}^{-3}$, NMB = -8.1%) compared to the default configuration
471 (MB = $-0.54 \mu\text{g m}^{-3}$, NMB = -25.7%). Compared to the standalone TM5-MP
472 simulation with the VBS configuration, MB and NMB are lower, whereas MAGE and
473 NME are higher (MAGE = $0.94 \mu\text{g m}^{-3}$, NME = 44.5%). This mainly indicates that
474 the additional SOA-iv production in EC-Earth, resulting from differences in
475 meteorological treatment, further reduces systematic errors but increases bias and
476 scatter.

477 Figure 7e shows the annual cycle of monthly mean $\text{PM}_{2.5}$ OA concentrations
478 at EMEP and IMPROVE sites in the TM5-MP offline and EC-Earth simulations
479 during 2005. For TM5-MP, the VBS configuration predicts higher concentrations
480 throughout the year compared to the default configuration. However, $\text{PM}_{2.5}$ OA is still
481 underpredicted, particularly at European sites and during winter. The same applies for
482 EC-Earth simulations. Because of the limited availability of European sites during
483 2005 (only 3 stations), EC-Earth online simulations were also evaluated for 2010,
484 when data from 8 stations were available, providing a more robust evaluation of
485 European predictions considering that the differences in predicted OA concentrations
486 between online and offline (TM5-MP) simulations of EC-Earth are relatively small.
487 The VBS configuration of EC-Earth slightly reduces the underprediction of OA
488 concentrations in Europe (MB= $-1.88 \mu\text{g m}^{-3}$, NMB= -40.7%) compared to the
489 default configuration (MB= $-1.95 \mu\text{g m}^{-3}$, NMB= -42.4%) but the bias remains
490 substantial, especially during winter (Fig. 7e). This underestimation may result from
491 the omission of oxidation of biomass burning emissions by NO_3 radicals, as well as

Commented [SK27]: Reviewer 1 Comment 9

492 uncertainties in the biomass burning emissions themselves (Reddington et al., 2019;
493 Hua et al., 2024). ~~The same applies for EC-Earth simulations.~~

Commented [SK28]: Reviewer 1 Comment 8

Commented [SK29]: Reviewer 2 Comment 2

494 Despite uncertainties in the emissions for fuel combustion and biomass
495 burning, the predictions of OA concentrations using the VBS configuration show
496 improved performance and are generally in good agreement with measurements.
497 Please note that the formation of SOA from anthropogenic VOC emissions (to reduce
498 computational cost) and from oxidation by NO₃ radicals is neglected in the model,
499 which may partially explain the remaining bias. The previous study of Tsimpidi et al.
500 (2014) indicated that SOA from anthropogenic VOCs contributes only about 15% to
501 the global average surface OA concentration. Additionally, the absence of biogenic
502 SOA formation in the models from sesquiterpenes may also contribute to the
503 underprediction (Bergman et al., 2022; Dada et al., 2023).

504

505 4. Summary and conclusions

506 We have implemented a lite configuration of the ORACLE module into the TM5-MP
507 CTM, which represents the chemistry-transport component of the EC-Earth3-
508 AerChem ESM. This version of the module applies the VBS framework to simulate
509 SOA formation from LVOCs, SVOCs, and IVOCs.

510 ~~The incorporation of ORACLE-lite reduced the bias of the OA predictions~~
511 ~~both in the offline and online simulations of EC-Earth3-AerChem. The incorporation~~
512 ~~of ORACLE lite significantly improved the representation of OA formation and~~
513 ~~atmospheric behavior both in the standalone TM5-MP and the EC-Earth.~~

Commented [SK30]: Reviewer 1 Comment 10

514 The models evaluation against monthly measured PM_{2.5} OA concentrations from Europe (EMEP)
515 and US (IMPROVE) stations indicated that OA concentrations were generally
516 underpredicted. However, the VBS configuration reduced NMB by nearly half in
517 TM5-MP and a factor of three in EC-Earth and improved the overall agreement.
518 There is a remaining NMB in both models (-13% in TM5-MP and -8% in EC-Earth)
519 which can be explained by the absence of SOA formation from anthropogenic VOC
520 emissions and sesquiterpenes or via oxidation by NO₃ radicals, which can be subjects
521 for future work. Compared to the traditional POA (default) configuration, the VBS
522 implementation increased the global annual mean surface OA concentration in TM5-
523 MP by 25% to 1.07 μg m⁻³ and the atmospheric OA burden by 50%, to 3.67 Tg.
524 Corresponding predictions from EC-Earth were slightly higher, with a surface OA

525 concentration of $1.16 \mu\text{g m}^{-3}$ and an atmospheric burden of 3.83 Tg, representing
526 increases of 30% and 60%, respectively. These changes resulted primarily from the
527 inclusion of SOA production from S/IVOCs and the treatment of gas-particle
528 partitioning and chemical aging, processes absent in the default OA scheme.

529 Our results indicate that SOA is the dominant contributor to total OA surface
530 concentrations and atmospheric burden, whereas POA contributes less than 30% to
531 both, highlighting the importance of including gas-phase oxidation and partitioning of
532 OA in ESMs. ~~The seasonal and spatial variability of SOA was also better captured,
533 with higher concentrations predicted in regions with intense biomass burning and
534 anthropogenic activity, such as India, China, and sub-Saharan Africa.~~

Commented [SK31]: Reviewer 1 Comment 11

535 Overall, the lite configuration of ORACLE module captures well the key
536 processes driving OA formation and evolution, offering a more realistic simulation of
537 OA concentrations without significantly increasing computational cost
538 (approximately 8%). This efficient and robust configuration supports future studies on
539 the climatic impacts of OA within ESMs.

540

541 **Acknowledgments**

542 This work was supported by the REINFORCE research project, implemented in the
543 framework of HFRI called “Basic Research Financing (Horizontal Support of all
544 Sciences)” under the National Recovery and Resilience Plan “Greece 2.0” funded by
545 the European Union - Next Generation EU (HFRI project no. 15155). We also
546 acknowledge support by the project Atmospheric nanoparticles, air quality and human
547 health (NANOSOMs) funded by the Hellenic Foundation for Research and Innovation
548 (HFRI) (grant no. 11504). Computational time was granted from the National
549 Infrastructures for Research and Technology S.A. (GRNET S.A.) in the National HPC
550 facility – ARIS – under project ID 010003 (AEROSIM). Acknowledgement is made
551 for the use of ECMWF's computing and archive facilities in this research (Special
552 Project: EC-Earth Atmospheric Composition developments).

553

554 **Code availability**

555 The EC-Earth3-AerChem code (version 3.5.0) is available to members of the EC-
556 Earth consortium via the EC-Earth development portal (<https://dev.ec-earth.org/>, last
557 accessed: 12 November 2025). Model components developed at ECMWF, such as the
558 IFS atmospheric model, are the intellectual property of ECMWF and its member

559 states. Access to the EC-Earth3-AerChem version 3.5.0 source code can be requested
560 through the EC-Earth website (<http://www.ec-earth.org/>, last accessed: 12 November
561 2025) and may be granted upon signing a software license agreement with ECMWF.
562 Due to licensing restrictions, access is currently limited to European users. ~~The post-~~
563 ~~processing scripts used for creating the main figures of the manuscript are available at~~
564 ~~Zenodo (<https://doi.org/10.5281/zenodo.18255310>).~~ ~~The code developed in this~~
565 ~~study and all relevant features, including the ORACLE v1.0 module and~~
566 ~~ISORROPIA-lite as part of the EC-Earth, are archived with a restricted access doi~~
567 ~~(<https://doi.org/10.5281/zenodo.19186090>) and have already been incorporated into~~
568 ~~the official development branch of EC-Earth3, making them part of future released~~
569 ~~versions. The TMS MP version 1.2 code with modifications for the VBS framework~~
570 ~~of this work can be found at Zenodo (<https://doi.org/10.5281/zenodo.18254761>). The~~
571 ~~lite configuration of the ORACLE v1.0 code, which is part of the ECHAM/MESSy~~
572 ~~Atmospheric Chemistry (EMAC) model, can be obtained by applying for an EMAC~~
573 ~~license, or upon request by emailing A. Tsimpidi (a.tsimpidi@fz-juelich.de).~~ ~~More~~
574 ~~information can be found on the MESSy Consortium website ([https://isorroopia.epfl.ch](http://www.messy-
575 interface.org). ISORROPIA lite is available upon request at <a href=).~~
576 ~~Post processing scripts used for creating the main figures of the manuscript are~~
577 ~~available at Zenodo (<https://doi.org/10.5281/zenodo.18255310>).~~

Field Code Changed

Commented [SK32]: Chief Editor Comment 2

Field Code Changed

579 Data availability

580 The data used for the model evaluation ~~in Figs. 7 and 8~~ are from two freely available
581 observational networks: the United States Interagency Monitoring of Protected Visual
582 Environments (IMPROVE; <https://views.cira.colostate.edu/fed/QueryWizard/>, last
583 access: 2 June 2025) ~~for fine organic mass in the IMPROVE Aerosol dataset~~ and the
584 European Monitoring and Evaluation Project (EMEP; [data.nilu.no/Default.aspx](https://ebas-
585 <a href=), last access: 2 June 2025). ~~The monthly measurements of~~
586 ~~PM_{2.5} OA from EMEP and IMPROVE networks used in this study are available at:~~
587 ~~<https://doi.org/10.5281/zenodo.19185962>.~~ ~~for PM_{2.5} organic carbon in the EMEP~~
588 ~~framework.~~ The data produced in the study are available from the authors upon
589 request.

Commented [SK33]: Chief Editor Comment 3

591 Competing interests

592 The authors declare that they have no conflicts of interest.

593

594 **Author contributions**

595 SK contributed to the implementation of the ORACLE-lite module into the model,
596 conducted the CTM simulations, analyzed the results, and wrote the paper. SM
597 designed the study, integrated the ORACLE-lite code into the model, conducted the
598 ESM simulations, and also contributed to writing the paper. APT and VAK provided
599 the ORACLE-lite code, supported its integration into the model, and contributed to
600 manuscript preparation. SNP supervised the study and contributed to manuscript
601 writing.

602

603 **References**

- 604 Aiken, A. C., DeCarlo, P. F., Kroll, J. H., Worsnop, D. R., Huffman, J. A., Docherty,
605 K. S., Ulbrich, I. M., Mohr, C., Kimmel, J. R., Sueper, D., Sun, Y., Zhang, Q.,
606 Trimborn, A., Northway, M., Ziemann, P. J., Canagaratna, M. R., Onasch, T.
607 B., Alfarra, M. R., Prevot, A. S. H., Dommen, J., Duplissy, J., Metzger, A.,
608 Baltensperger, U., and Jimenez, J. L.: O/C and OM/OC ratios of primary,
609 secondary, and ambient organic aerosols with high-resolution time-of-flight
610 aerosol mass spectrometry, *Environ. Sci. Technol.*, 42, 4478–4485, doi:
611 10.1021/es703009q, 2008.
- 612 Aiken, A. C., Salcedo, D., Cubison, M. J., Huffman, J. A., DeCarlo, P. F., Ulbrich, I.
613 M., Docherty, K. S., Sueper, D., Kimmel, J. R., Worsnop, D. R., Trimborn, A.,
614 Northway, M., Stone, E. A., Schauer, J. J., Volkamer, R. M., Fortner, E., de
615 Foy, B., Wang, J., Laskin, A., Shutthanandan, V., Zheng, J., Zhang, R.,
616 Gaffney, J., Marley, N. A., Paredes-Miranda, G., Arnott, W. P., Molina, L. T.,
617 Sosa, G., and Jimenez, J. L.: Mexico City aerosol analysis during MILAGRO
618 using high resolution aerosol mass spectrometry at the urban supersite (T0) –
619 Part 1: Fine particle composition and organic source apportionment, *Atmos.*
620 *Chem. Phys.*, 9, 6633–6653, doi:10.5194/acp-9-6633-2009, 2009.
- 621 Balsamo, G., Viterbo, P., Beijaars, A., van den Hurk, B., Hirschi, M., Betts, A. K.,
622 and Scipal, K.: A revised hydrology for the ECMWF model: Verification from
623 field site to terrestrial water storage and impact in the integrated forecast
624 system, *J. Hydrometeorol.*, 10, 623–643, doi: 10.1175/2008JHM1068.1, 2009.
- 625 Bergman, T., Makkonen, R., Schrödner, R., Swietlicki, E., Phillips, V. T. J., Le Sager,
626 P., and van Noije, T.: Description and evaluation of a secondary organic

627 aerosol and new particle formation scheme within TM5-MP v1.2, *Geosci.*
628 *Model Dev.*, 15, 683–713, doi:10.5194/gmd-15-683-2022, 2022.

629 Bergström, R., Denier van der Gon, H. A. C., Prévôt, A. S. H., Yttri, K. E., and
630 Simpson, D.: Modelling of organic aerosols over Europe (2002–2007) using a
631 volatility basis set (VBS) framework: application of different assumptions
632 regarding the formation of secondary organic aerosol, *Atmos. Chem. Phys.*,
633 12, 8499–8527, doi: 10.5194/acp-12-8499-2012, 2012.

634 Bougiatioti, A., Nikolaou, P., Stavroulas, I., Kouvarakis, G., Weber, R., Nenes, A.,
635 Kanakidou, M., and Mihalopoulos, N.: Particle water and pH in the eastern
636 Mediterranean: source variability and implications for nutrient availability,
637 *Atmos. Chem. Phys.*, 16, 4579–4591, doi: 10.5194/acp-16-4579-2016, 2016.

638 Chen, X., Yang, W., Wang, Z., Li, J., Hu, M., An, J., Wu, Q., Wang, Z., Chen, H.,
639 and Wei, Y.: Improving new particle formation simulation by coupling a
640 volatility-basis set (VBS) organic aerosol module in NAQPMS+APM, *Atmos.*
641 *Environ.*, 204, 1–11, doi: 10.1016/j.atmosenv.2019.01.053, 2019.

642 Craig, A., Valcke, S., and Coquart, L.: Development and performance of a new
643 version of the OASIS coupler, OASIS3-MCT_3.0, *Geosci. Model Dev.*, 10,
644 3297–3308, doi: 10.5194/gmd-10-3297-2017, 2017.

645 Crippa, M., Canonaco, F., Slowik, J. G., El Haddad, I., DeCarlo, P. F., Mohr, C.,
646 Heringa, M. F., Chirico, R., Marchand, N., Temime-Roussel, B., Abidi, E.,
647 Poulain, L., Wiedensohler, A., Baltensperger, U., and Prévôt, A. S. H.:
648 Primary and secondary organic aerosol origin by combined gas-particle phase
649 source apportionment, *Atmos. Chem. Phys.*, 13, 8411–8426, doi: 10.5194/acp-
650 13-8411-2013, 2013.

651 Dada, L., Stolzenburg, D., Simon, M., Fischer, L., Heinritzi, M., Wang, M., Xiao, M.,
652 Vogel, A. L., Ahonen, L., Amorim, A., Baalbaki, R., Baccharini, A.,
653 Baltensperger, U., Bianchi, F., Daellenbach, K. R., DeVivo, J., Dias, A.,
654 Dommen, J., Duplissy, J., Finkenzeller, H., Hansel, A., He, X-C.,
655 Hofbauer, V., Hoyle, C. R., Kangasluoma, J., Kim, C., Kürten, A.,
656 Kvashnin, A., Mauldin, R., Makhmutov, V., Marten, R., Mentler, B., Nie, W.,
657 Petäjä, T., Quéléver, L. L. J., Saathoff, H., Tauber, C., Tome, A., Molteni, U.,
658 Volkamer, R., Wagner, R., Wagner, A. C., Wimmer, D., Winkler, P. M.,
659 Yan, C., Zha, Q., Rissanen, M., Gordon, H., Curtius, J., Worsnop, D. R.,
660 Lehtipalo, K., Donahue, N. M., Kirkby, J., El Haddad, I., and Kulmala, M.:

661 Role of sesquiterpenes in biogenic new particle formation, *Sci. Adv.*, 9, 36,
662 doi:10.1126/sciadv.adi5297, 2023.

663 Dee, D. P., Uppala, S. M., Simmons, A. J., Berrisford, P., Poli, P., Kobayashi, S.,
664 Andrae, U., Balmaseda, M. A., Balsamo, G., Bauer, P., Bechtold, P., Beljaars,
665 A. C. M., van de Berg, L., Bidlot, J., Bormann, N., Delsol, C., Dragani, R.,
666 Fuentes, M., Geer, A. J., Haimberger, L., Healy, S. B., Hersbach, H., Hólm,
667 E. V., Isaksen, I., Kållberg, P., Köhler, M., Matricardi, M., McNally, A. P.,
668 Monge-Sanz, B. M., Morcrette, J.-J., Park, B.-K., Peubey, C., de Rosnay, P.,
669 Tavolato, C., Thépaut, J.-N., and Vitart, F.: The ERA-Interim reanalysis:
670 configuration and performance of the data assimilation system, *Q. J. Roy.*
671 *Meteor. Soc.*, 137, 553–597, doi: 10.1002/qj.828, 2011.

672 Donahue, N. M., Robinson, A. L., Stanier, C. O., and Pandis, S. N.: Coupled
673 partitioning, dilution, and chemical aging of semivolatile organics, *Environ.*
674 *Sci. Technol.*, 40, 2635–2643, 2006.

675 Döscher, R., Acosta, M., Alessandri, A., Anthoni, P., Arsouze, T., Bergman, T.,
676 Bernardello, R., Boussetta, S., Caron, L.-P., Carver, G., Castrillo, M.,
677 Catalano, F., Cvijanovic, I., Davini, P., Dekker, E., Doblas-Reyes, F. J.,
678 Docquier, D., Echevarria, P., Fladrich, U., Fuentes-Franco, R., Gröger, M., v.
679 Hardenberg, J., Hieronymus, J., Karami, M. P., Keskinen, J.-P., Koenigk, T.,
680 Makkonen, R., Massonnet, F., Ménégos, M., Miller, P. A., Moreno-Chamarro,
681 E., Nieradzic, L., van Noije, T., Nolan, P., O'Donnell, D., Ollinaho, P., van
682 den Oord, G., Ortega, P., Prims, O. T., Ramos, A., Reerink, T., Rousset, C.,
683 Ruprich-Robert, Y., Le Sager, P., Schmith, T., Schrödner, R., Serva, F.,
684 Sicardi, V., Sloth Madsen, M., Smith, B., Tian, T., Tourigny, E., Uotila, P.,
685 Vancoppenolle, M., Wang, S., Wårlind, D., Willén, U., Wyser, K., Yang, S.,
686 Yepes-Arbós, X., and Zhang, Q.: The EC-Earth3 Earth system model for the
687 Coupled Model Intercomparison Project 6, *Geosci. Model Dev.*, 15, 2973–
688 3020, doi: 10.5194/gmd-15-2973-2022, 2022.

689 Eyring, V., Bony, S., Meehl, G. A., Senior, C. A., Stevens, B., Stouffer, R. J., and
690 Taylor, K. E.: Overview of the Coupled Model Intercomparison Project Phase
691 6 (CMIP6) experimental design and organization, *Geosci. Model Dev.*, 9,
692 1937–1958, doi:10.5194/gmd-9-1937-2016, 2016.

693 Fang, Z., Li, C., He, Q., Czech, H., Gröger, T., Zeng, J., Fang, H., Xiao, S., Pardo, M.,
694 Hartner, E., Meidan, D., Wang, X., Zimmermann, R., Laskin, A., and Rudich,

695 Y.: Secondary organic aerosols produced from photochemical oxidation of
696 secondarily evaporated biomass burning organic gases: Chemical composition,
697 toxicity, optical properties, and climate effect, *Environ. Int.*, 157, 106801, doi:
698 10.1016/j.envint.2021.106801, 2021.

699 Gao, C. Y., Bauer, S. E., Tsigaridis, K., and Im, U.: Global influence of organic
700 aerosol volatility on aerosol microphysical processes: Composition and
701 number, *Journal of Advances in Modeling Earth Systems*, 16,
702 e2023MS004185, doi: 10.1029/2023MS004185, 2024.

703 Grieshop, A. P., Logue, J. M., Donahue, N. M., and Robinson, A. L.: Laboratory
704 investigation of photochemical oxidation of organic aerosol from wood fires 1:
705 measurement and simulation of organic aerosol evolution, *Atmos. Chem.*
706 *Phys.*, 9, 1263–1277, doi: 10.5194/acp-9-1263-2009, 2009.

707 Heald, C. L., Jacob, D. J., Park, R. J., Russell, L. M., Huebert, B. J., Seinfeld, J. H.,
708 Liao, H., and Weber, R. J.: A large organic aerosol source in the free
709 troposphere missing from current models, *Geophys. Res. Lett.*, 32, L18809,
710 doi: 10.1029/2005gl023831, 2005.

711 Hennigan, C. J., Miracolo, M. A., Engelhart, G. J., May, A. A., Presto, A. A., Lee, T.,
712 Sullivan, A. P., McMeeking, G. R., Coe, H., Wold, C. E., Hao, W.-M.,
713 Gilman, J. B., Kuster, W. C., de Gouw, J., Schichtel, B. A., Collett Jr., J. L.,
714 Kreidenweis, S. M., and Robinson, A. L.: Chemical and physical
715 transformations of organic aerosol from the photo-oxidation of open biomass
716 burning emissions in an environmental chamber, *Atmos. Chem. Phys.*, 11,
717 7669–7686, doi:10.5194/acp-11-7669-2011, 2011.

718 Hildebrandt, L., Engelhart, G. J., Mohr, C., Kostenidou, E., Lanz, V. A., Bougiatioti,
719 A., DeCarlo, P. F., Prevot, A. S. H., Baltensperger, U., Mihalopoulos, N.,
720 Donahue, N. M., and Pandis, S. N.: Aged organic aerosol in the Eastern
721 Mediterranean: the Finokalia Aerosol Measurement Experiment – 2008,
722 *Atmos. Chem. Phys.*, 10, 4167–4186, doi:10.5194/acp-10-4167-2010, 2010.

723 Hu, W., Hu, M., Hu, W., Jimenez, J. L., Yuan, B., Chen, W., Wang, M., Wu, Y.,
724 Chen, C., Wang, Z., Peng, J., Zeng, L., and Shao, M.: Chemical composition,
725 sources and aging process of sub-micron aerosols in Beijing: contrast between
726 summer and winter, *J. Geophys. Res.-Atmos.*, 121, 1955–1977, doi:
727 10.1002/2015JD024020, 2016.

728 Hua, W., Lou, S., Huang, X., Xue, L., Ding, K., Wang, Z., and Ding, A.: Diagnosing
729 uncertainties in global biomass burning emission inventories and their impact
730 on modeled air pollutants, *Atmos. Chem. Phys.*, 24, 6787–6807, doi:
731 10.5194/acp-24-6787-2024, 2024.

732 Huijnen, V., Williams, J., van Weele, M., van Noije, T., Krol, M., Dentener, F.,
733 Segers, A., Houweling, S., Peters, W., de Laat, J., Boersma, F., Bergamaschi,
734 P., van Velthoven, P., Le Sager, P., Eskes, H., Alkemade, F., Scheele, R.,
735 Nédélec, P., and Pätz, H.-W.: The global chemistry transport model TM5:
736 description and evaluation of the tropospheric chemistry version 3.0, *Geosci.*
737 *Model Dev.*, 3, 445–473, doi: 10.5194/gmd-3-445-2010, 2010.

738 IPCC: Climate Change 2021: The Physical Science Basis. Working Group I
739 Contribution to the Sixth Assessment Report of the Intergovernmental Panel
740 on Climate Change, edited by: Masson-Delmotte, V., Zhai, P., Pirani, A.,
741 Connors, S. L., Péan, C., Berger, S., Caud, N., Chen, Y., Goldfarb, L., Gomis,
742 M. I., Huang, M., Leitzell, K., Lonnoy, E., Matthews, J. B. R., Maycock, T.
743 K., Waterfield, T., Yelekçi, O., Yu, R., and Zhou, B., Cambridge University
744 Press, Cambridge, United Kingdom and New York, NY, USA,
745 doi:10.1017/9781009157896, 2391 pp., 2021.

746 Irfan, M., Kühn, T., Yli-Juuti, T., Laakso, A., Holopainen, E., Worsnop, D. R.,
747 Virtanen, A., and Kokkola, H.: A model study investigating the sensitivity of
748 aerosol forcing to the volatilities of semi-volatile organic compounds, *Atmos.*
749 *Chem. Phys.*, 24, 8489–8506, doi: 10.5194/acp-24-8489-2024, 2024.

750 Jathar, S. H., Farina, S. C., Robinson, A. L., and Adams, P. J.: The influence of semi-
751 volatile and reactive primary emissions on the abundance and properties of
752 global organic aerosol, *Atmos. Chem. Phys.*, 11, 7727–7746, doi:10.5194/acp-
753 11-7727-2011, 2011.

754 Jiang, J., Aksoyoglu, S., El-Haddad, I., Ciarelli, G., Denier van der Gon, H. A. C.,
755 Canonaco, F., Gilardoni, S., Paglione, M., Minguillón, M. C., Favez, O.,
756 Zhang, Y., Marchand, N., Hao, L., Virtanen, A., Florou, K., O'Dowd, C.,
757 Ovadnevaite, J., Baltensperger, U., and Prévôt, A. S. H.: Sources of organic
758 aerosols in Europe: a modeling study using CAMx with modified volatility
759 basis set scheme, *Atmos. Chem. Phys.*, 19, 15247–15270, doi: 10.5194/acp-
760 19-15247-2019, 2019.

761 Jöckel, P., Tost, H., Pozzer, A., Brühl, C., Buchholz, J., Ganzeveld, L., Hoor, P.,
762 Kerkweg, A., Lawrence, M. G., Sander, R., Steil, B., Stiller, G., Tanarhte, M.,
763 Taraborrelli, D., van Aardenne, J., and Lelieveld, J.: The atmospheric
764 chemistry general circulation model ECHAM5/MESy1: consistent
765 simulation of ozone from the surface to the mesosphere, *Atmos. Chem. Phys.*,
766 6, 5067–5104, doi:10.5194/acp-6-5067-2006, 2006.

767 Kakavas, S., Pandis, S. N., and Nenes, A.: ISORROPIA-lite: A comprehensive
768 atmospheric aerosol thermodynamics module for Earth System Models, *Tellus*
769 B, 74, 1–23, 2022.

770 Kanakidou, M., Seinfeld, J. H., Pandis, S. N., Barnes, I., Dentener, F. J., Facchini, M.
771 C., Van Dingenen, R., Ervens, B., Nenes, A., Nielsen, C. J., Swietlicki, E.,
772 Putaud, J. P., Balkanski, Y., Fuzzi, S., Horth, J., Moortgat, G. K.,
773 Winterhalter, R., Myhre, C. E. L., Tsigaridis, K., Vignati, E., Stephanou, E.
774 G., and Wilson, J.: Organic aerosol and global climate modelling: a review,
775 *Atmos. Chem. Phys.*, 5, 1053–1123, doi: 10.5194/acp-5-1053-2005, 2005.

776 Krol, M., Houweling, S., Bregman, B., van den Broek, M., Segers, A., van Velthoven,
777 P., Peters, W., Dentener, F., and Bergamaschi, P.: The two-way nested global
778 chemistry-transport zoom model TM5: algorithm and applications, *Atmos.*
779 *Chem. Phys.*, 5, 417–432, doi: 10.5194/acp-5-417-2005, 2005.

780 Kroll, J. H. and Seinfeld, J. H.: Chemistry of secondary organic aerosol: Formation
781 and evolution of low-volatility organics in the atmosphere, *Atmos. Environ.*,
782 42, 3593–3624, 2008.

783 Lim, C. Y., Hagan, D. H., Coggon, M. M., Koss, A. R., Sekimoto, K., de Gouw, J.,
784 Warneke, C., Cappa, C. D., and Kroll, J. H.: Secondary organic aerosol
785 formation from the laboratory oxidation of biomass burning emissions, *Atmos.*
786 *Chem. Phys.*, 19, 12797–12809, doi: 10.5194/acp-19-12797-2019, 2019.

787 Ma, P., Zhang, P., Shu, J., Yang, B., and Zhang, H.: Characterization of secondary
788 organic aerosol from photo-oxidation of gasoline exhaust and specific sources
789 of major components, *Environ. Pollut.*, 232, 65–72, doi:
790 10.1016/j.envpol.2017.09.018, 2018.

791 Monks, P., Granier, C., Fuzzi, S., Stohl, A., Williams, M., Akimoto, H., Amann, M.,
792 Baklanov, A., Baltensperger, U., Bey, I., Blake, N., Blake, R., Carslaw, K.,
793 Cooper, O., Dentener, F., Fowler, D., Fragkou, E., Frost, G., Generoso, S.,
794 Ginoux, P., Grewe, V., Guenther, A., Hansson, H., Henne, S., Hjorth, J.,

795 Hofzumahaus, A., Huntrieser, H., Isaksen, I., Jenkin, M., Kaiser, J.,
796 Kanakidou, M., Klimont, Z., Kulmala, M., Laj, P., Lawrence, M., Lee, J.,
797 Liousse, C., Maione, M., McFiggans, G., Metzger, A., Mieville, A.,
798 Moussiopoulos, N., Orlando, J., O'Dowd, C., Palmer, P., Parrish, D., Petzold,
799 A., Platt, U., Pöschl, U., Prévôt, A., Reeves, C., Reimann, S., Rudich, Y.,
800 Sellegri, K., Steinbrecher, R., Simpson, D., ten Brink, H., Theloke, J., van der
801 Werf, G., Vautard, R., Vestreng, V., Vlachokostas, C., and von Glasow, R.:
802 Atmospheric composition change – global and regional air quality, *Atmos.*
803 *Environ.*, 43, 5268–5350, doi: 10.1016/j.atmosenv.2009.08.021, 2009.

804 Myriokefalitakis, S., Bergas-Massó, E., Gonçalves-Ageitos, M., Pérez García-Pando,
805 C., van Noije, T., Le Sager, P., Ito, A., Athanasopoulou, E., Nenes, A.,
806 Kanakidou, M., Krol, M. C., and Gerasopoulos, E.: Multiphase processes in
807 the EC-Earth model and their relevance to the atmospheric oxalate, sulfate,
808 and iron cycles, *Geosci. Model Dev.*, 15, 3079–3120, doi: 10.5194/gmd-15-
809 3079-2022, 2022.

810 Nault, B. A., Campuzano-Jost, P., Day, D. A., Schroder, J. C., Anderson, B.,
811 Beyersdorf, A. J., Blake, D. R., Brune, W. H., Choi, Y., Corr, C. A., de Gouw,
812 J. A., Dibb, J., DiGangi, J. P., Diskin, G. S., Fried, A., Huey, L. G., Kim, M.
813 J., Knote, C. J., Lamb, K. D., Lee, T., Park, T., Pusede, S. E., Scheuer, E.,
814 Thornhill, K. L., Woo, J.-H., and Jimenez, J. L.: Secondary organic aerosol
815 production from local emissions dominates the organic aerosol budget over
816 Seoul, South Korea, during KORUS-AQ, *Atmos. Chem. Phys.*, 18, 17769–
817 17800, doi: 10.5194/acp-18-17769-2018, 2018.

818 Pai, S. J., Heald, C. L., Pierce, J. R., Farina, S. C., Marais, E. A., Jimenez, J. L.,
819 Campuzano-Jost, P., Nault, B. A., Middlebrook, A. M., Coe, H., Shilling, J.
820 E., Bahreini, R., Dingle, J. H., and Vu, K.: An evaluation of global organic
821 aerosol schemes using airborne observations, *Atmos. Chem. Phys.*, 20, 2637–
822 2665, doi: 10.5194/acp-20-2637-2020, 2020.

823 Pandis, S. N., Wexler, A. S., and Seinfeld, J. H.: Secondary organic aerosol formation
824 and transport. 2. Predicting the ambient secondary organic aerosol-size
825 distribution, *Atmos. Environ. AGen.*, 27, 2403–2416, 1993.

826 Pandis, S. N., Donahue, N. M., Murphy, B. N., Riipinen, I., Fountoukis, C., Karnezi,
827 E., Patoulias, D., and Skyllakou, K.: Introductory lecture: atmospheric organic
828 aerosols: insights from the combination of measurements and chemical

829 transport models, *Faraday Discussion*, 165, 9–24, doi: 10.1039/c3fd00108c,
830 2013.

831 Pitchford, M., Malm, W., Schichtel, B., Kumar, N., Lowenthal, D., and Hand, J.:
832 Revised Algorithm for Estimating Light Extinction from IMPROVE Particle
833 Speciation Data, *J. Air Waste Manage.*, 57, 1326–1336, doi: 10.3155/1047-
834 3289.57.11.1326, 2007.

835 Reddington, C. L., Morgan, W. T., Darbyshire, E., Brito, J., Coe, H., Artaxo, P.,
836 Scott, C. E., Marsham, J., and Spracklen, D. V.: Biomass burning aerosol over
837 the Amazon: analysis of aircraft, surface and satellite observations using a
838 global aerosol model, *Atmos. Chem. Phys.*, 19, 9125–9152, doi: 10.5194/acp-
839 19-9125-2019, 2019.

840 Reid, J. S., Koppmann, R., Eck, T. F., and Eleuterio, D. P.: A review of biomass
841 burning emissions part II: intensive physical properties of biomass burning
842 particles, *Atmos. Chem. Phys.*, 5, 799–825, doi: 10.5194/acp-5-799-2005,
843 2005.

844 Riipinen, I., Talvinen, S., Chassaing, A., Georgakaki P., Li, X., García-Pando, P. C.,
845 Bergman, T., Kommula, M. S., Proske, U., Gkouvousis, A., Tsimpidi, P. A.,
846 Chatziparaschos, M., Neuberger, A., Karydis, A. V., Calderón, M. S.,
847 Romakkaniemi, S., Partridge, G. D., Khadir, T., Dada, L., van Noije, T.,
848 Decesari, S., Seland, Ø., Zieger, P., Bender, F., Carlslaw, K., Cermak, J.,
849 Costa-Surós, M., Ageitos, M. G., Gramlich, Y., Haugvaldstad, W. O.,
850 Holopainen, E., Hoose, C., Jorba, O., Kakavas, S., Kanakidou, M., Kokkola,
851 H., Krehci, R., Kühn, T., Kulmala, M., La Sager, P., Makkonen, R., Manavi,
852 E. I. S., Mentel, F. T., Milousis, A., Myriokefalitakis, S., Nenes, A.,
853 Nieminen, T., Pandis, S. N., Patoulias, D., Petäjä, T., Quaas, J., Regayre, L.,
854 Scholz, M. C. S., Schulz, M., Skyllakou, K., Sousse, R., Stier, P., Thomas, M.
855 A., Villinger, J. T., Virtanen, A., Wyser, K., and Ekman, M. L. A.: Treatment
856 of Key Aerosol and Cloud Processes in Earth System Models –
857 Recommendations from the FORCeS Project, *Tellus B*, under revision, 2025.

858 Robinson, A. L., Donahue, N. M., Shrivastava, M. K., Weitkamp, E. A., Sage, A. M.,
859 Grieshop, A. P., Lane, T. E., Pierce, J. R., and Pandis, S. N.: Rethinking
860 organic aerosols: Semivolatile emissions and photochemical aging, *Science*,
861 315, 1259–1262, 2007.

862 Rousset, C., Vancoppenolle, M., Madec, G., Fichet, T., Flavoni, S., Barthélemy, A.,
863 Benshila, R., Chanut, J., Levy, C., Masson, S., and Vivier, F.: The Louvain-
864 La-Neuve sea ice model LIM3.6: global and regional capabilities, *Geosci.*
865 *Model Dev.*, 8, 2991–3005, doi: 10.5194/gmd-8-2991-2015, 2015.

866 Schauer, J. J., Kleeman, M. J., Cass, G. R., and Simoneit, B. R. T.: Measurement of
867 emissions from air pollution sources. 5. C₁-C₃₂ organic compounds from
868 gasoline-powered motor vehicles, *Environ Sci Technol*, 36, 1169–1180, doi:
869 10.1021/es0108077, 2002.

870 Sengupta, D., Samburova, V., Bhattarai, C., Watts, A. C., Moosmüller, H., and
871 Khlystov, A. Y.: Polar semivolatile organic compounds in biomass-burning
872 emissions and their chemical transformations during aging in an oxidation
873 flow reactor, *Atmos. Chem. Phys.*, 20, 8227–8250, doi: 10.5194/acp-20-8227-
874 2020, 2020.

875 Shrivastava, M., Fast, J., Easter, R., Gustafson Jr., W. I., Zaveri, R. A., Jimenez, J. L.,
876 Saide, P., and Hodzic, A.: Modeling organic aerosols in a megacity:
877 comparison of simple and complex representations of the volatility basis set
878 approach, *Atmos. Chem. Phys.*, 11, 6639–6662, doi: 10.5194/acp-11-6639-
879 2011, 2011.

880 Shrivastava, M., Cappa, C. D., Fan, J., Goldstein, A. H., Guenther, A. B.,
881 Jimenez, J. L., Kuang, C., Laskin, A., Martin, S. T., Ng, N. L., Petaja, T.,
882 Pierce, J. R., Rasch, P. J., Roldin, P., Seinfeld, J. H., Shilling, J., Smith, J. N.,
883 Thornton, J. A., Volkamer, R., Wang, J., Worsnop, D. R., Zaveri, R. A.,
884 Zelenyuk, A., and Zhang, Q.: Recent advances in understanding secondary
885 organic aerosol: implications for global climate forcing, *Rev. Geophys.*, 55,
886 509–559, doi: 10.1002/2016RG000540, 2017.

887 Spracklen, D. V., Jimenez, J. L., Carslaw, K. S., Worsnop, D. R., Evans, M. J., Mann,
888 G. W., Zhang, Q., Canagaratna, M. R., Allan, J., Coe, H., McFiggans, G., Rap,
889 A., and Forster, P.: Aerosol mass spectrometer constraint on the global
890 secondary organic aerosol budget, *Atmos. Chem. Phys.*, 11, 12109–12136,
891 doi: 10.5194/acp-11-12109-2011, 2011.

892 Taylor, K. E., Williamson, D., and Zwiers, F.: The sea surface temperature and sea ice
893 concentration boundary conditions for AMIP II simulations, *Progr. Clim.*
894 *Model Diagnosis Intercomp.*, PCMDI Report No. 60, 1–24

895 , <https://pcmdi.llnl.gov/report/pdf/60.pdf?id=42> (last access: 14 May 2025),
896 2000.

897 Tsigaridis, K., Daskalakis, N., Kanakidou, M., Adams, P. J., Artaxo, P., Bahadur, R.,
898 Balkanski, Y., Bauer, S. E., Bellouin, N., Benedetti, A., Bergman, T.,
899 Berntsen, T. K., Beukes, J. P., Bian, H., Carslaw, K. S., Chin, M., Curci, G.,
900 Diehl, T., Easter, R. C., Ghan, S. J., Gong, S. L., Hodzic, A., Hoyle, C. R.,
901 Iversen, T., Jathar, S., Jimenez, J. L., Kaiser, J. W., Kirkevåg, A., Koch, D.,
902 Kokkola, H., Lee, Y. H., Lin, G., Liu, X., Luo, G., Ma, X., Mann, G. W.,
903 Mihalopoulos, N., Morcrette, J.-J., Müller, J.-F., Myhre, G., Myriokefalitakis,
904 S., Ng, N. L., O'Donnell, D., Penner, J. E., Pozzoli, L., Pringle, K. J., Russell,
905 L. M., Schulz, M., Sciare, J., Seland, Ø., Shindell, D. T., Sillman, S., Skeie, R.
906 B., Spracklen, D., Stavrou, T., Steenrod, S. D., Takemura, T., Tiitta, P.,
907 Tilmes, S., Tost, H., van Noije, T., van Zyl, P. G., von Salzen, K., Yu, F.,
908 Wang, Z., Wang, Z., Zaveri, R. A., Zhang, H., Zhang, K., Zhang, Q., and
909 Zhang, X.: The AeroCom evaluation and intercomparison of organic aerosol
910 in global models, *Atmos. Chem. Phys.*, 14, 10845–10895, doi: 10.5194/acp-
911 14-10845-2014, 2014.

912 Tsimpidi, A. P., Karydis, V. A., Zavala, M., Lei, W., Molina, L., Ulbrich, I. M.,
913 Jimenez, J. L., and Pandis, S. N.: Evaluation of the volatility basis-set
914 approach for the simulation of organic aerosol formation in the Mexico City
915 metropolitan area, *Atmos. Chem. Phys.*, 10, 525–546, doi:10.5194/acp-10-
916 525-2010, 2010.

917 Tsimpidi, A. P., Karydis, V. A., Pozzer, A., Pandis, S. N., and Lelieveld, J.: ORACLE
918 (v1.0): module to simulate the organic aerosol composition and evolution in
919 the atmosphere, *Geosci. Model Dev.*, 7, 3153–3172, doi: 10.5194/gmd-7-
920 3153-2014, 2014.

921 Tsimpidi, A. P., Karydis, V. A., Pandis, S. N., and Lelieveld, J.: Global combustion
922 sources of organic aerosols: model comparison with 84 AMS factor-analysis
923 data sets, *Atmos. Chem. Phys.*, 16, 8939–8962, doi: 10.5194/acp-16-8939-
924 2016, 2016.

925 Tsimpidi, A. P., Karydis, V. A., Pandis, S. N., and Lelieveld, J.: Global-scale
926 combustion sources of organic aerosols: sensitivity to formation and removal
927 mechanisms, *Atmos. Chem. Phys.*, 17, 7345–7364, doi: 10.5194/acp-17-7345-
928 2017, 2017.

929 Tsimpidi, A. P., Scholz, S. M. C., Milousis, A., Mihalopoulos, N., and Karydis, V. A.:
930 Aerosol composition trends during 2000–2020: in-depth insights from model
931 predictions and multiple worldwide near-surface observation datasets, *Atmos.*
932 *Chem. Phys.*, 25, 10183–10213, doi: 10.5194/acp-25-10183-2025, 2025.

933 Turpin, B. J. and Lim, H.-J.: Species contributions to PM_{2.5} mass concentrations:
934 Revisiting common assumptions for estimating organic mass, *Aerosol Sci.*
935 *Technol.*, 35, 602–610, doi: 10.1080/02786820119445, 2001.

936 Vancoppenolle, M., Fichet, T., Goosse, H., Bouillon, S., Madec, G., and Maqueda,
937 M. A. M.: Simulating the mass balance and salinity of Arctic and Antarctic sea
938 ice. 1. Model description and validation, *Ocean Model.*, 27, 33–53, doi:
939 10.1016/j.ocemod.2008.10.005, 2009.

940 van Noije, T., Le Sager, P., Segers, A. J., van Velthoven, P. F. J., Krol, M. C.,
941 Hazeleger, W., Williams, A. G., and Chambers, S. D.: Simulation of
942 tropospheric chemistry and aerosols with the climate model EC-Earth, *Geosci.*
943 *Model Dev.*, 7, 2435–2475, doi: 10.5194/gmd-7-2435-2014, 2014.

944 van Noije, T., Bergman, T., Le Sager, P., O'Donnell, D., Makkonen, R., Gonçalves-
945 Ageitos, M., Döscher, R., Fladrich, U., von Hardenberg, J., Keskinen, J.-P.,
946 Korhonen, H., Laakso, A., Myriokefalitakis, S., Ollinaho, P., Pérez García-
947 Pando, C., Reerink, T., Schrödner, R., Wyser, K., and Yang, S.: EC-Earth3-
948 AerChem: a global climate model with interactive aerosols and atmospheric
949 chemistry participating in CMIP6, *Geosci. Model Dev.*, 14, 5637–5668, doi:
950 10.5194/gmd-14-5637-2021, 2021.

951 Vignati, E., Wilson, J., and Stier, P.: M7: An efficient size-resolved aerosol
952 microphysics module for large-scale aerosol transport models, *J. Geophys.*
953 *Res.*, 109, D22202, doi: 10.1029/2003JD004485, 2004.

954 Williams, J. E., Boersma, K. F., Le Sager, P., and Verstraeten, W. W.: The high-
955 resolution version of TM5-MP for optimized satellite retrievals: description
956 and validation, *Geosci. Model Dev.*, 10, 721–750, doi: 10.5194/gmd-10-721-
957 2017, 2017.

958 Woody, M. C., Baker, K. R., Hayes, P. L., Jimenez, J. L., Koo, B., and Pye, H. O. T.:
959 Understanding sources of organic aerosol during CalNex-2010 using the
960 CMAQ-VBS, *Atmos. Chem. Phys.*, 16, 4081–4100, doi: 10.5194/acp-16-
961 4081-2016, 2016.

962 Yarwood, G., Rao, S., Yocke, M., and Whitten, G. Z.: Updates to the Carbon Bond
963 Chemical Mechanism: CB05, Research Triangle
964 Park, https://www.camx.com/Files/CB05_Final_Report_120805.pdf (last
965 access: April 2025), 2005.

966 Zhang, Q., Jimenez, J. L., Canagaratna, M. R., Allan, J. D., Coe, H., Ulbrich, I.,
967 Alfarra, M. R., Takami, A., Middlebrook, A. M., Sun, Y. L., Dzepina, K.,
968 Dunlea, E., Docherty, K., DeCarlo, P. F., Salcedo, D., Onasch, T., Jayne, J. T.,
969 Miyoshi, T., Shimo, A., Hatakeyama, S., Takegawa, N., Kondo, Y.,
970 Schneider, J., Drewnick, F., Borrmann, S., Weimer, S., Demerjian, K.,
971 Williams, P., Bower, K., Bahreini, R., Cottrell, L., Griffin, R. J., Rautiainen,
972 J., Sun, J. Y., Zhang, Y. M., and R., W. D.: Ubiquity and dominance of
973 oxygenated species in organic aerosols in anthropogenically-influenced
974 Northern Hemisphere midlatitudes, *Geophys. Res. Lett.*, 34, L13801, doi:
975 10.1029/2007GL029979, 2007.

976 Zhang, B.: The effect of aerosols to climate change and society, *J. Geosci. Environ.*
977 *Protect.*, 8, 55, doi: 10.4236/gep.2020.88006, 2020.

978
979
980
981
982
983
984
985
986
987
988
989
990
991
992
993

994 **Table 1:** Overview of the ORACLE-lite module characteristics, including volatility
 995 classification, evolution processes, and OA formation types for each emission
 996 class

Emissions	C* ($\mu\text{g m}^{-3}$)	Initial Representative volatility bin ($\mu\text{g m}^{-3}$)	Evolution in ORACLE-lite	OA type
LVOCs	10^{-2} - 10^{-1}	10^{-2}	Gas/particle partitioning	POA
SVOCs	10^0 - 10^2	10^1	Gas/particle partitioning and aging	POA and SOA
IVOCs	10^3 - 10^6	10^4	Aging and gas/particle partitioning	SOA
VOCs	$>10^6$	$>10^6$	Aging and gas/particle partitioning	SOA

Commented [SK34]: Reviewer 2 Comment 9

997
 998
 999
 1000
 1001
 1002
 1003
 1004
 1005
 1006
 1007
 1008
 1009
 1010
 1011
 1012
 1013
 1014
 1015
 1016
 1017
 1018

1019 **Table 2:** Global budgets, atmospheric burdens and lifetimes of **(a)** POA, **(b)** SOA-sv,
 1020 **(c)** SOA-iv, **(d)** bSOA-v for EC-Earth during 2000-2010 and TM5-MP during
 1021 2005 with the VBS configuration

	EC-Earth (2000-2010)	TM5-MP (2005)
LVOCs emissions (Tg yr ⁻¹)	7.40±3.98	7.54
SVOCs emissions (Tg yr ⁻¹)	31.42±10.89	31.81
IVOCs emissions (Tg yr ⁻¹)	52.78±9.34	53.13
(a) POA		
Evaporation (Tg yr ⁻¹)	3.57±0.35	3.81
Dry deposition (Tg yr ⁻¹)	3.48±0.79	3.26
Wet deposition (Tg yr ⁻¹)	31.70±8.52	31.58
Atmospheric burden (Tg)	0.73±0.04	0.69
Lifetime (days)	6.85	6.49
(b) SOA-sv		
Production (Tg yr ⁻¹)	19.62±1.67	19.83
Dry deposition (Tg yr ⁻¹)	2.02±0.17	1.97
Wet deposition (Tg yr ⁻¹)	17.56±2.63	17.41
Atmospheric burden (Tg)	0.60±0.03	0.60
Lifetime (days)	11.13	11.38
(c) SOA-iv		
Production (Tg yr ⁻¹)	38.28±7.32	37.02
Dry deposition (Tg yr ⁻¹)	3.90±0.57	3.37
Wet deposition (Tg yr ⁻¹)	34.26±6.39	32.39
Atmospheric burden (Tg)	1.35±0.07	1.21
Lifetime (days)	12.92	12.33
(d) bSOA-v		
Production (Tg yr ⁻¹)	51.31±1.24	52.34
Dry deposition (Tg yr ⁻¹)	0.69±0.07	0.40
Wet deposition (Tg yr ⁻¹)	50.67±6.70	50.58
Atmospheric burden (Tg)	1.15±0.06	1.18
Lifetime (days)	8.19	8.42

1022

1023 **Table 3:** Evaluation metrics comparing monthly averaged predicted PM_{2.5} OA
 1024 concentrations with IMPROVE and EMEP observations for the simulations of
 1025 TM5-MP and EC-Earth ~~during 2005~~

Commented [SK35]: Reviewer 1 Comment 8

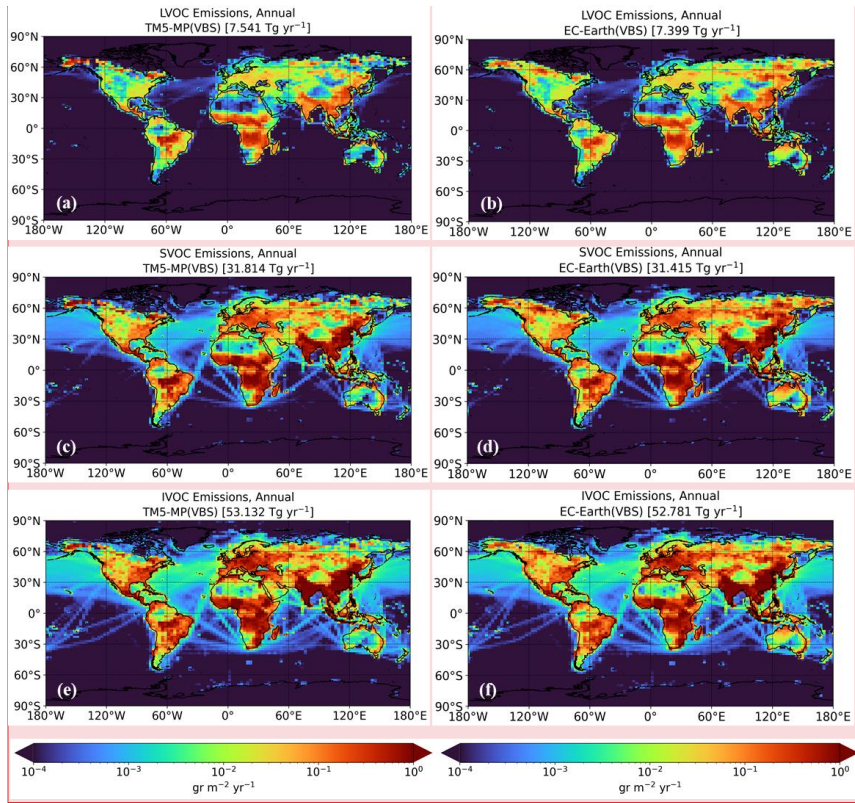
Commented [SK36]: Reviewer 2 Comment 2

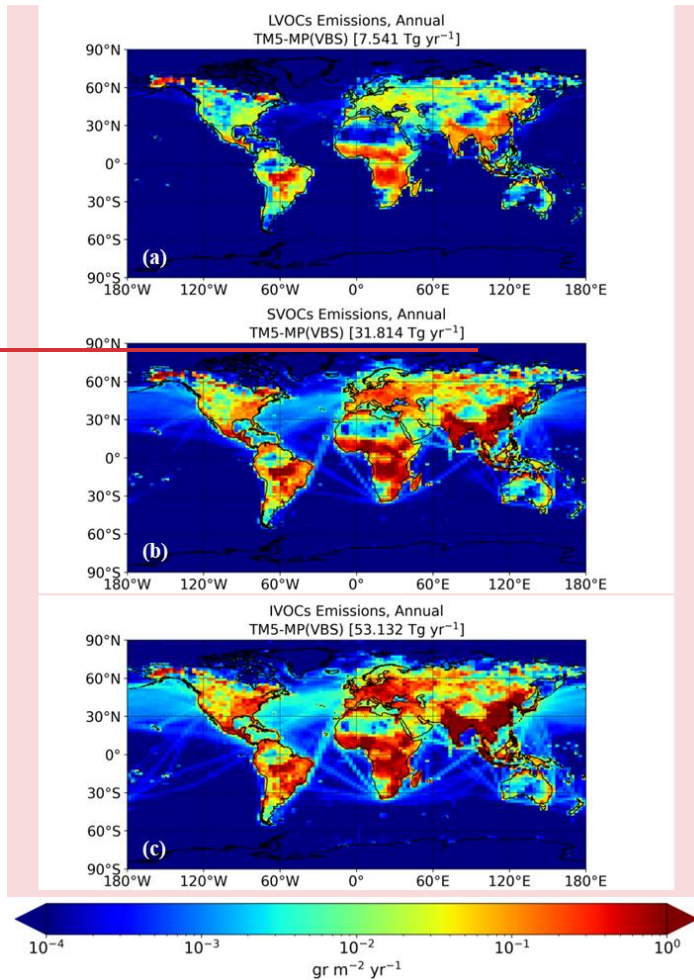
Simulations	Number of measurements	Mean observed ($\mu\text{g m}^{-3}$)	Mean predicted ($\mu\text{g m}^{-3}$)	MB ($\mu\text{g m}^{-3}$)	MAGE ($\mu\text{g m}^{-3}$)	NMB (%)	NME (%)	RMSE ($\mu\text{g m}^{-3}$)
IMPROVE and EMEP during 2005								
TM5-MP (Default)	2124	2.11	1.54	-0.57	0.89	-27.1	42.0	1.57
TM5-MP (VBS)	2124	2.11	1.83	-0.28	0.82	-13.2	38.9	1.50
EC-Earth (Default)	2124	2.11	1.57	-0.54	0.96	-25.7	45.6	1.68
EC-Earth (VBS)	2124	2.11	1.94	-0.17	0.94	-8.1	44.5	1.61
EMEP during 2010								
<u>EC-Earth (Default)</u>	<u>95</u>	<u>4.61</u>	<u>2.66</u>	<u>-1.95</u>	<u>2.57</u>	<u>-42.4</u>	<u>55.8</u>	<u>4.24</u>
<u>EC-Earth (VBS)</u>	<u>95</u>	<u>4.61</u>	<u>2.73</u>	<u>-1.88</u>	<u>2.51</u>	<u>-40.7</u>	<u>54.5</u>	<u>4.4</u>

Commented [SK37]: Reviewer 2 Comment 2

Commented [SK38]: Reviewer 1 Comment 8

1026
 1027
 1028
 1029
 1030
 1031
 1032
 1033
 1034
 1035
 1036
 1037





1039

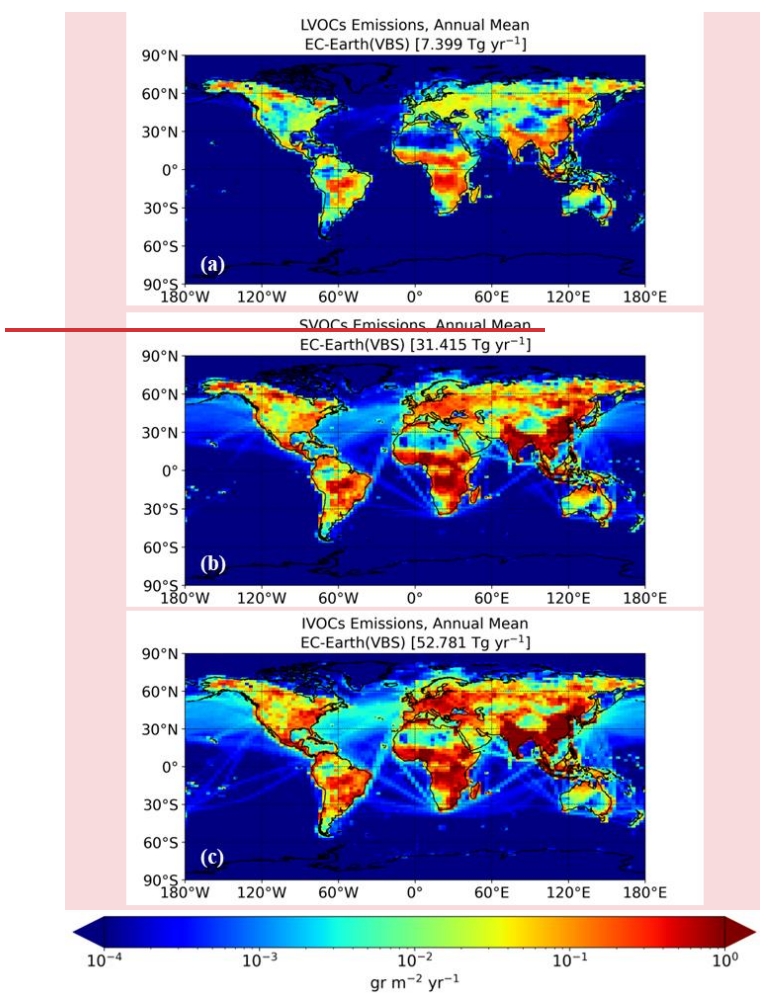
1040 **Figure 1.** Annual emissions (in $\text{gr m}^{-2} \text{yr}^{-1}$) applied in the simulations of TM5-MP
 1041 during 2005 (left column) and EC-Earth during 2000-2010 (right column) for: (a), (b)
 1042 low volatile organic compounds (LVOCs), (c), (d) semi-volatile organic compounds
 1043 (SVOCs), and (e), (f) intermediate volatile organic compounds (IVOCs). Annual
 1044 emissions (in $\text{gr m}^{-2} \text{yr}^{-1}$) of: (a) low volatile organic compounds (LVOCs), (b) semi-
 1045 volatile organic compounds (SVOCs), and (c) intermediate volatile organic
 1046 compounds (IVOCs) applied in the standalone TM5-MP simulation during 2005.

1047

1048

1049

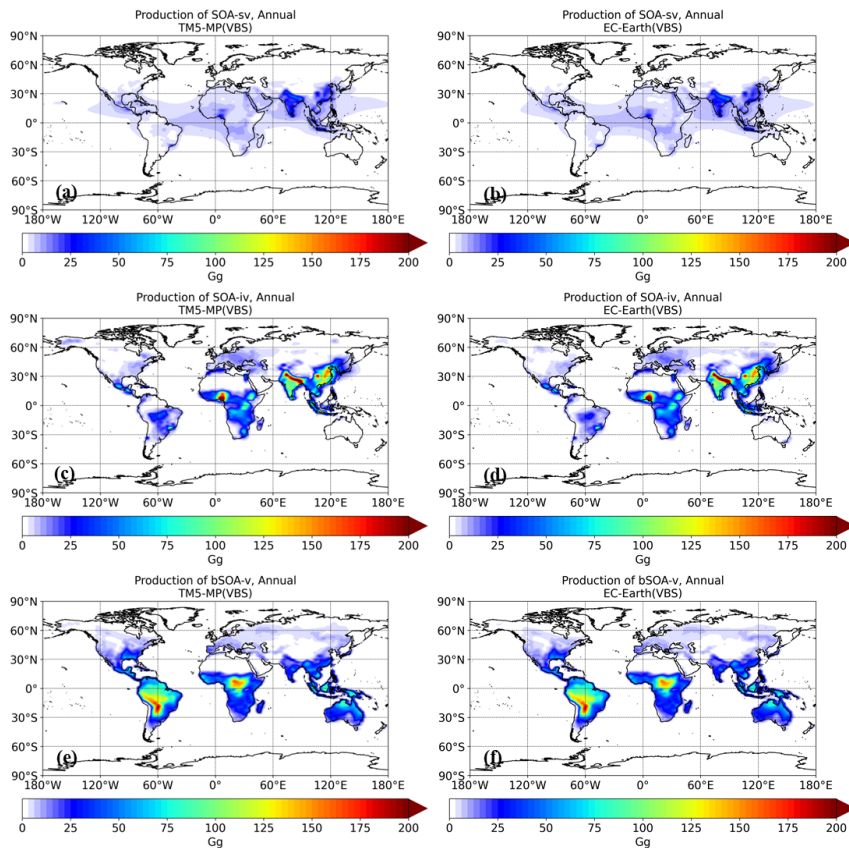
1050
1051
1052



1053
1054
1055
1056
1057
1058

Figure 2. Annual mean emissions (in $\text{gr m}^{-2} \text{yr}^{-1}$) of: (a) low volatile organic compounds (LVOCs), (b) semi volatile organic compounds (SVOCs), and (c) intermediate volatile organic compounds (IVOCs) applied in the EC Earth simulation during 2000-2010.

Commented [SK39]: Reviewer 1 Comment 9



1059

1060 **Figure 32.** Annual production of SOA (in Gg) as simulated using the VBS
 1061 configuration of TM5-MP during 2005 (left column) and the corresponding EC-Earth
 1062 predictions during 2000-2010 (right column) for: (a), (b) SOA-sv, and (c), (d) SOA-
 1063 iv. For completeness, annual SOA production from biogenic VOCs (bSOA-v) in
 1064 panels (e) and (f) is also shown.

1065

1066

1067

1068

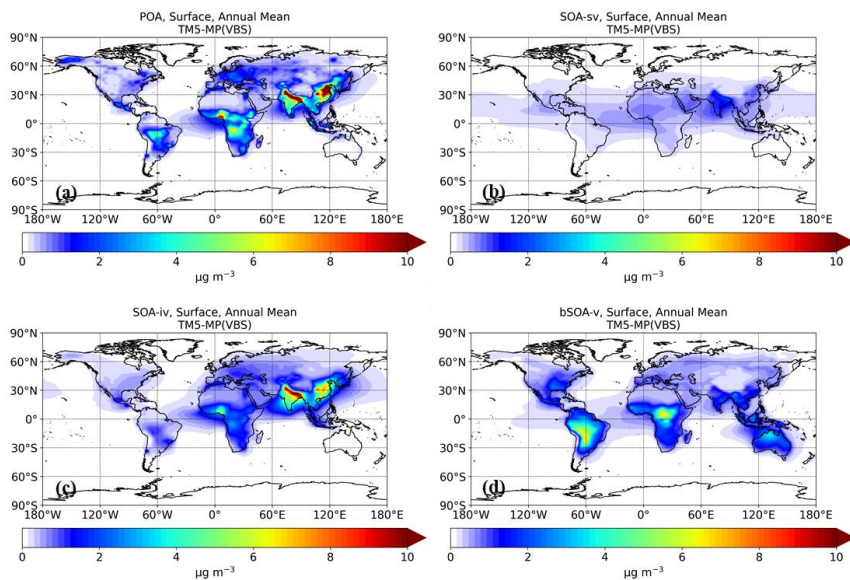
1069

1070

1071

1072

Commented [SK40]: Reviewer 1 Comment 9



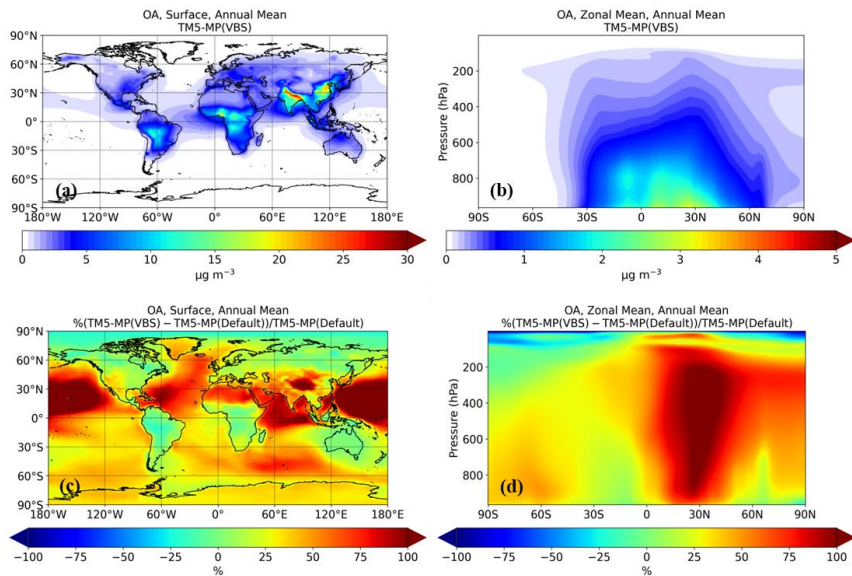
1073

1074 **Figure 34.** Annual mean surface concentrations (in $\mu\text{g m}^{-3}$) of: **(a)** POA, **(b)** SOA
 1075 from SVOCs (SOA-sv), and **(c)** SOA from IVOCs (SOA-iv) as simulated using the
 1076 VBS configuration of TM5-MP during 2005. For completeness, SOA concentrations
 1077 from biogenic VOCs (bSOA-v) in panel **(d)** are also shown.

1078

1079

Commented [SK41]: Reviewer 1 Comment 9



1080

1081 **Figure 45.** Annual mean concentrations of total organic aerosol (in $\mu\text{g m}^{-3}$): (a)
 1082 surface concentrations, and (b) zonal values as simulated using the VBS configuration
 1083 of TM5-MP during 2005. Panels (c) and (d) show the corresponding relative
 1084 differences (in %) compared to the previous (default) model configuration. A positive
 1085 change indicates that the VBS configuration predicts more than the default.

1086

1087

1088

1089

1090

1091

1092

1093

1094

1095

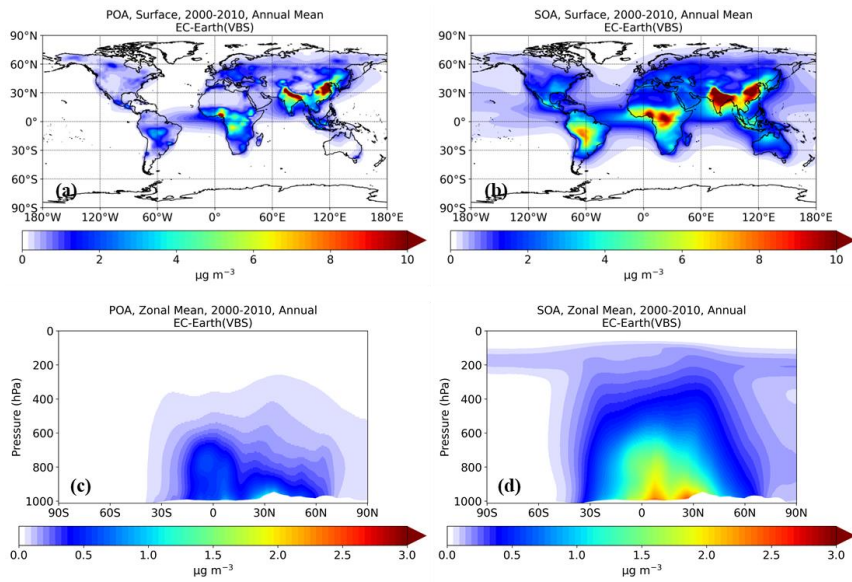
1096

1097

1098

1099

Commented [SK42]: Reviewer 1 Comment 9



1100

1101 **Figure 65.** Annual mean concentrations of POA and SOA (in $\mu\text{g m}^{-3}$): (a), (b) surface
 1102 concentrations, and (c), (d) zonal values as simulated using the VBS configuration of
 1103 EC-Earth during 2000-2010.

1104

1105

1106

1107

1108

1109

1110

1111

1112

1113

1114

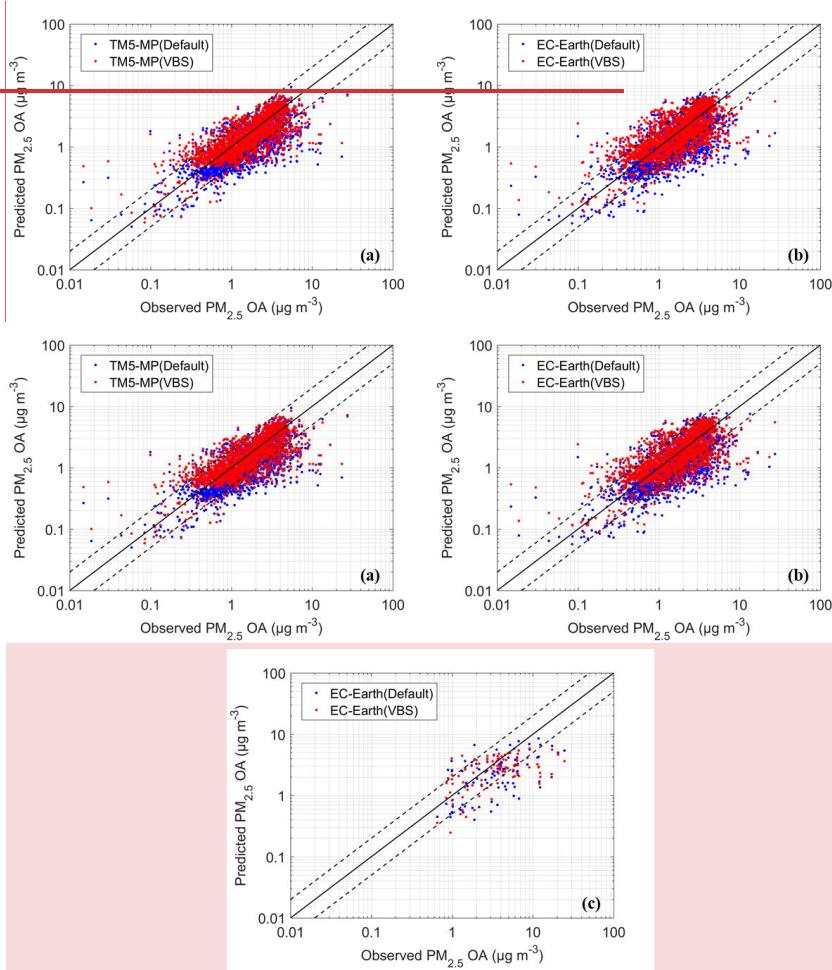
1115

1116

1117

Commented [SK43]: Reviewer 1 Comment 9

1118



1119

1120 **Figure 76.** Organic mass concentrations from simulations of: (a) TM5-MP during
1121 2005, and (b) EC-Earth during 2005, and (c) EC-Earth during 2010. Scatterplots of
1122 the first row compare predicted PM_{2.5} OA concentrations (in µg m⁻³) with
1123 observations from both the IMPROVE and EMEP monitoring networks, while the
1124 second row shows a single comparison only with EMEP. Models' results are shown
1125 for the default configuration (blue) and the VBS configuration (red). Each point
1126 represents a monthly average value at a monitoring site.

1127

1128

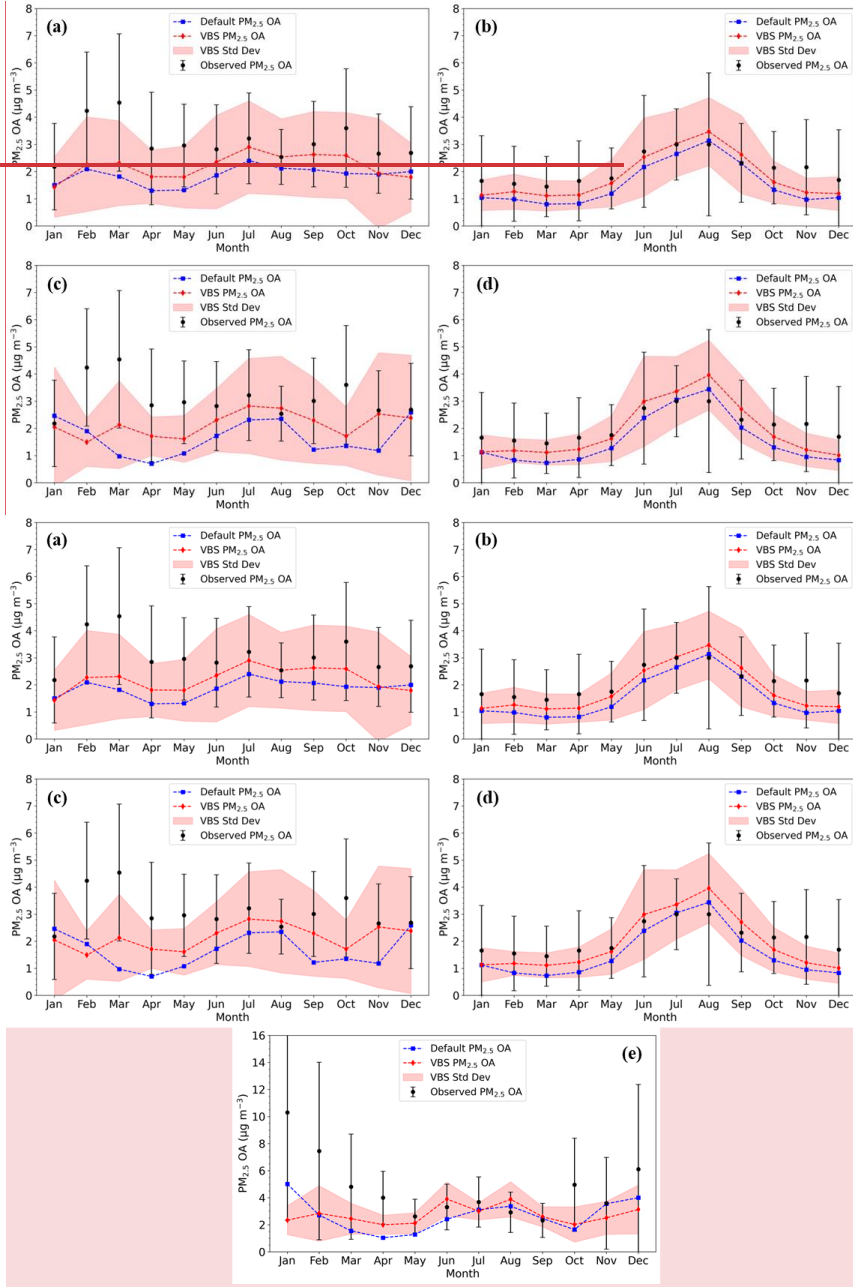
Commented [SK44]: Reviewer 1 Comment 9

Commented [SK45]: Reviewer 1 Comment 8

Commented [SK46]: Reviewer 2 Comment 2

1129
1130
1131
1132
1133
1134
1135
1136
1137
1138
1139
1140

1141



1142

1143 **Figure 78.** Annual cycles of monthly mean PM_{2.5} OA concentrations during 2005.

Commented [SK47]: Reviewer 1 Comment 9

1144 The top row shows results from the standalone TM5-MP simulations at: (a) EMEP
 1145 sites and (b) IMPROVE sites during 2005; while the bottom-middle row shows

1146 results from the EC-Earth simulation at: **(c)** EMEP sites and **(d)** IMPROVE sites
1147 during 2005; and panel (e) shows results from the EC-Earth simulation at EMEP sites
1148 during 2010. The red line represents the mean predicted by the VBS simulation, with
1149 red shading indicating the standard deviation. The blue line represents the mean
1150 predicted by the default simulation. Black dots show the observed mean values, with
1151 vertical lines showing the corresponding standard deviations.

1152

Commented [SK48]: Reviewer 1 Comment 8

Commented [SK49]: Reviewer 2 Comment 2